Chapter 1
INTRODUCTION

The application of thermal sciences is not only limited to common engineering scenarios but is being potentially extended to realms which have not been envisaged earlier. One such modern application, which has come to the fore, is in the analysis and prediction of thermal behavior of infrared (IR) detector cryochamber. Infrared detectors are devices, which are highly sensitive to temperature and require special cryochambers for housing them for their optimal functioning. Prior to discussing the details of infrared detectors and manner in which thermal analysis of cryochambers may be carried out, the first few sessions briefly dwell on infrared radiation and history of IR detectors for the sake of completeness and better comprehension.

1.1 Infrared (IR) radiation and its fundamentals

The Latin prefix "infra" means "below" or "beneath." Infrared radiations are radiations below (infra) visible spectrum. This emergent dual use technology field is fast emerging amongst the most ubiquitous ones.

"Infrared" refers to the region beyond or beneath the red end of the visible color spectrum. The infrared region is located between the visible and microwave regions of the electromagnetic spectrum. Because heated objects radiate energy in the infrared, it is often referred to as the heat region of the spectrum. Infrared radiation is popularly known as "heat" or sometimes known as "heat radiation", since many people attribute all radiant heating to infrared light and/or all infrared radiation to heating. This is a widespread misconception, since light and electromagnetic waves of any frequency will heat surfaces that absorb them. Infrared light from the Sun only accounts for 49% of the heating of the Earth, with the rest being caused by visible light that is absorbed then re-radiated at longer wavelengths. All objects radiate some energy in the infrared region which even includes objects at room temperature and frozen objects such as ice.

Some characteristics of infrared radiation are that it travels basically in a straight line (although some exceptions to this are important in our work), does not penetrate

metals unless they are very thin, and passes through many crystalline, plastic, and gaseous materials- including the earth's atmosphere.

Infrared (IR) radiation is a form of radiated electromagnetic energy, obeying the same laws as those for visible light, radio waves and X-rays. In fact, its only fundamental difference from those forms of electromagnetic radiation is its wavelength. This is shown in the chart of electromagnetic spectrum in fig (1.1). The borderlines between visible, infrared, far-infrared, and millimeter waves are not absolute. These areas of the spectrum have been segregated primarily for convenience in discussions; the primary criteria are the sources used and the detectors that are available.

Normal light is generally understood to be that portion of the spectrum to which the human eye is sensitive. While, millimeter waves are the shortest wavelengths that can be received with the smallest microwave like apparatus, and infrared and the far infrared are the wavelengths falling in between.

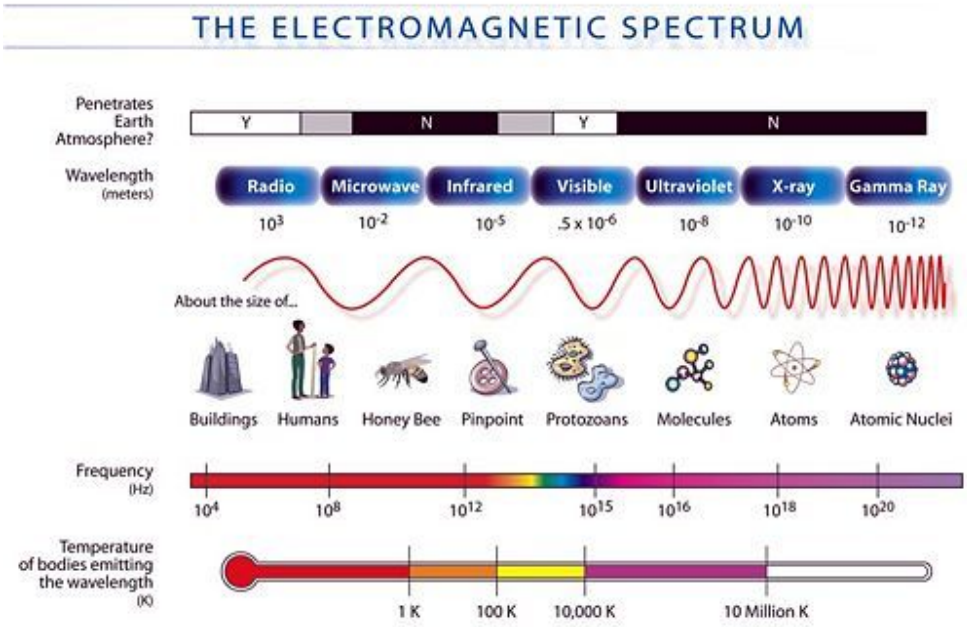

Fig (1.1): Electromagnetic Spectrum

Most of the IR detectors take advantage of two atmospheric "windows"- spectral regions that transmit well: the 3-5μm window and 8-12μm window. Thus, we could

include the 3 to 12μm region as primary IR region [1]. IR methods work with wavelengths as low as 0.7μm and as high as 1000μm.

Various authors have published different proposals of division of IR range. However, the typical division is shown below (Table 1).

Region (abbreviation)	Wavelength range (μm)
Near Infrared (NIR)	0.78-1
Short Wavelength IR (SWIR)	1-3
Medium Wavelength IR (MWIR)	3-6
Long Wavelength IR (LWIR)	6-15
Very long Wavelength IR (VLWIR)	15-1000

Table (1.1): Classification of infrared radiation

1.2 Applications of Infrared (IR) Imaging and detection

Ever since astronomer Sir William Herschel in April 1800 announced the discovery of, which we now understand as infra red (IR) portion of spectrum, development of IR engineering progressed in tandem with IR detectors. He experimented with a thermometer as a detector to measure the distribution of energy in sunlight. Following the works of Kirchhoff, Stefan Boltzmann, Wien, and Rayleigh, Max Planck culminated the effort with the well-known Planck's law. Although, earliest applications of IR dealt with detection of IR radiation, later applications matured to newer detectors and their exploitation by forming IR arrays.

Infrared (IR) detectors have been called the *eyes of the digital battlefield.* Military applications in western countries have spearheaded and dominated the requirements in this field akin to many other emerging fields. In addition to many military applications for IR systems such as target acquisition, search and track, missile seeker guidance, there is a great potential for IR systems in commercial market because the military market is decreasing and concurrently becoming more specialized. Today, only about 20% of the market is commercial. After a decade the commercial market is estimated to grow by over 70% in volume and 40% in value [2].

Non-military uses include thermal efficiency analysis, remote temperature sensing, short-ranged wireless communication, spectroscopy, and weather forecasting.

Infrared astronomy uses sensor-equipped telescopes to penetrate dusty regions of space, such as molecular clouds; detect objects such as planets, and to view highly red-shifted objects from the early days of the universe.

An infrared detector is simply a transducer of radiant energy, converting radiant energy in the infrared into a measurable form. Since infrared radiation does not rely on visible light, it offers the possibility of seeing in the dark or through obscured conditions, by detecting the infrared energy emitted by objects. The detected energy is translated into imagery showing the energy differences between objects, thus allowing an otherwise obscured scene to be seen.

Under infrared light, the world reveals features not apparent under regular visible light [3]. People and animals are easily seen in total darkness, weaknesses are revealed in structures, components close to failure glow brighter, visibility is improved in adverse condition such as smoke or fog.

For example, in the fig (1.2), the left image below is what you may see in ordinary light on a dark night. The image at right is the same scene but as seen with an infrared camera. It is apparent that hot objects such as people stand out from the typically cooler backgrounds regardless of the available visible light. This kind of detection is possible employing suitable IR cameras and can be useful in various kinds of combat scenarios.

a) Image as seen under ordinary light

b) Same image scene as in (a) seen under infrared camera

Fig (1.2): Comparison of ordinary imaging (a) versus infrared imaging

1.3 Need for cooling

Almost all Infrared (IR) detectors are cooled, mostly to cryogenic temperatures, below −150 °C, −238 °F or 123 K, either because they will not operate at room temperature or because they operate much better when cooled. However, the necessity to operate in such cryogenic regimes makes the application of IR detectors extremely complex. This also demands a through thermal analysis in determining the necessary cooling load specific to the application since these detectors will also interact thermally with the environment. This is also essential in order to design most appropriate cooling methodologies suitable for specific scenarios.

1.4 Scope of work

The scope of the present work involves the thorough study of thermal conditions and phenomenon essential for optimal operation of IR detectors and transducers. An overall qualitative analysis of the design considerations of a cryochamber / Dewar housing these IR devices has been carried out which include; mechanical design considerations, need of vacuum integrity, applicable refrigeration systems. Further, finite volume analysis for better comprehending the thermal phenomenon arising in the cryochamber has also been carried out. The modeling results have been subsequently validated through experiments on similar systems to establish its efficacy.

Chapter 2
LITERATURE REVIEW

There are two fundamental methods of IR detection, Thermal (energy) and Quantum (photon) detection. Thermal detectors respond to temperature changes generated from incident IR radiation through changes in material properties and do not require cooling. Quantum detectors generate free electrical carriers through the interaction of photons and bound electrons. Energy detectors are low cost and typically used in single detector applications; common applications include fire detection systems and automatic light switches. In thermal imaging and range finding systems quantum detectors, which require cooling are used and offer high detection performance and a faster response speed. Thus a presence of a cooling system along with quantum detector based detection is mandatory. The literature survey of this area of cooling an IR detector is briefly described below.

Infrared (IR) sensors and focal plane arrays (FPAs) are widely used in ballistic missile defense (BMD). Tidrow & Dyer [4] presented an overview of the state of the art of IR sensors, and the advantages and shortfalls of each IR material system for BMD and space based applications. Important FPA characteristics for future BMD FPAs include large format, high sensitivity, low noise, good uniformity, and high operability.

The means to attain and maintain the vacuum necessary to maximize thermal insulation inside a cryochamber is discussed by Boffito et.al [5]. In particular, the characteristics and use of special non-evaporable getters, as well as their sorption behavior was investigated. Authors have described vacuum as an ideal thermal insulator, since the molecular thermal conductivity is minimized. Additional improvements in cutting thermal losses are often obtained with the use of reflecting shields (eg., Al foils, separated by thin insulators such as fibre glass sheets) to reduce another source of insulation loss, i.e., radiation. Heat inleak was found for a stainless steel (SS) Dewar (with the following dimensions: L=300mm, ϕ_e= 58mm, and ϕ_i= 38mm) filled with liquid nitrogen (LN_2), with only the evacuated jacket and with the use of reflecting multilayers (five Al foils 0.1 mm thick separated by four fiberglass sheets 0.2 mm thick). It was seen

that to have good insulation the vacuum should be better than ~10^{-1}or 10Pa (with multilayers). The multilayers further improve final insulation with respect to vacuum alone. Other losses depend on contacts and thus on the type of cryochamber. In order to maintain vacuum during life, which can be deteriorated not only by outgassing, but also by small leaks, which are difficult to measure, sorption means i.e., getters are introduced into the evacuated jacket. They are usually based on physical adsorption (such as zeolites), but some are based on chemical conversion of gases (essentially H_2, such as in case of using PdO). The characteristics of "chemical absorbers", i.e., the non-evaporable getters, have been investigated here considering a further important practical aim for the use of getters: to create an insitu pumping which helps improve and shorten baking process time.

Kang et.al [6] conducted an experimental study on transient cooling characteristics by changing inside pressure of infrared detector cryochamber. The experimental setup employed is as shown in fig (2.1). A vacuum pump was used to create the desired vacuum inside the chamber. Since temperature difference along the cooling area of bore was large, four temperature sensors were installed with 10mm gap. Liquid nitrogen was used for cooling the infrared sensor. The authors figured out characteristics

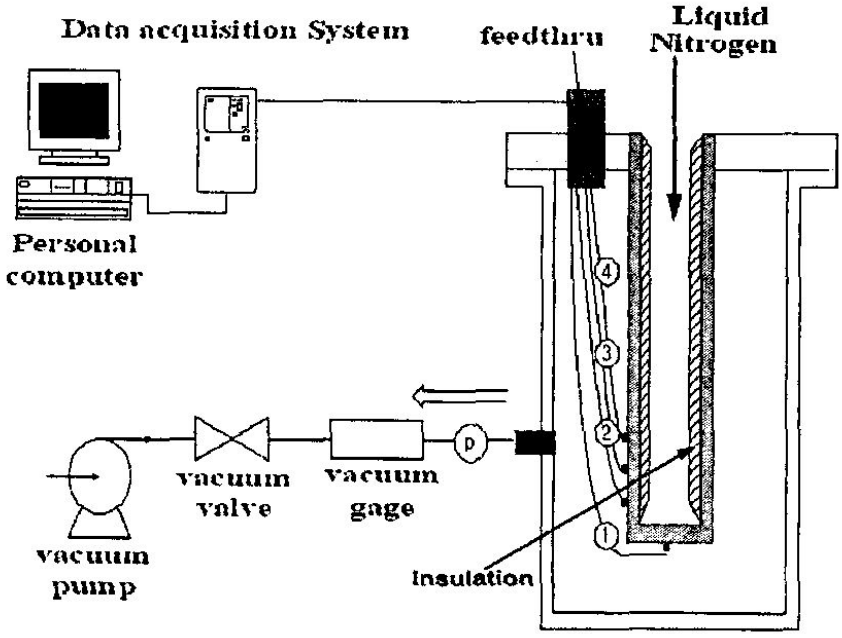

Fig (2.1): Schematic of the infrared detector cryochamber experimental setup

of heat transfer in transition state and temperature change of bore by changing pressure in chamber from ambient pressure to 50 Torr, 1 Torr and 0.1 Torr. The pressure in chamber mostly affected cooling time and heat inflow. It was observed that when the chamber was below 1 Torr, characteristics of temperature were unaffected and were very similar. Above the pressure of 1 Torr natural convection mostly affected cooling time and heat inflow.

Kim et.al [7] investigated steady cooling characteristics of a cryochamber analytically considering radiation shields. Cryochamber was modeled in two ways viz., in one, radiation shield installed only at detector, and in other, radiation shield installed both in detector and cold finger part. Schematic diagram for the variants is shown in fig (2.2).

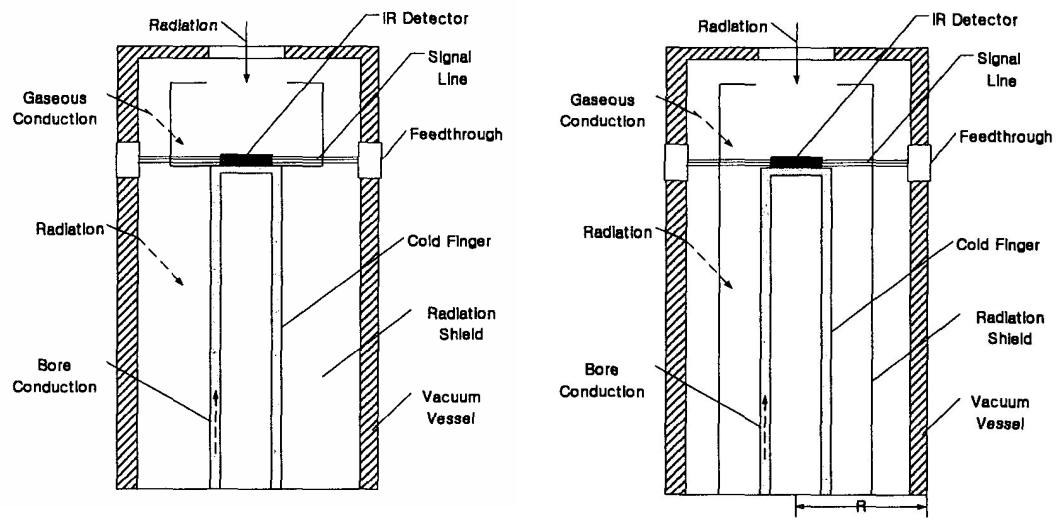

a) Installation of a radiation shield only in detector part

b) Installation of a radiation shield both in detector and cold finger part

Fig (2.2) Schematic diagram of cryochamber with radiation shield

Heat transfer in infrared sensor detector cryochamber with radiation shield was analyzed. It was observed that 97% heat inflow came through cold finger. Heat transfer in case of radiation shield at detector and cold finger decreased 26% at 10^{-5} torr and 12% at 1 torr in comparison to when radiation shield was present only at detector area. Above the inner pressure of 10^{-3} torr, heat inflow increased dramatically due to convective heat transfer inside the chamber. It was concluded that in order to minimize heat inflow, inside

inner pressure is to be maintained below 10^{-3} torr and radiation shield must be used to prevent heat inflow through cold finger.

Kim et.al [8] made an experimental study on the thermal loads of a cryochamber with a radiation shield. The schematic and shape of cryochamber for infrared sensor was similar to one shown in fig (2.2) without the radiation shield. Cooling load of the chamber was measured using an experimental setup, which consisted of turbo-molecular pump to create vacuum and a liquid nitrogen injector to make low temperature area freeze. In order to measure temperature at the end of low temperature, silicon diode temperature sensor was used. Further, in order to develop heat load on to the low temperature area, heating strip such as shown in fig (2.3) was wound at the end of low temperature area to conduct heat when power was supplied from outside.

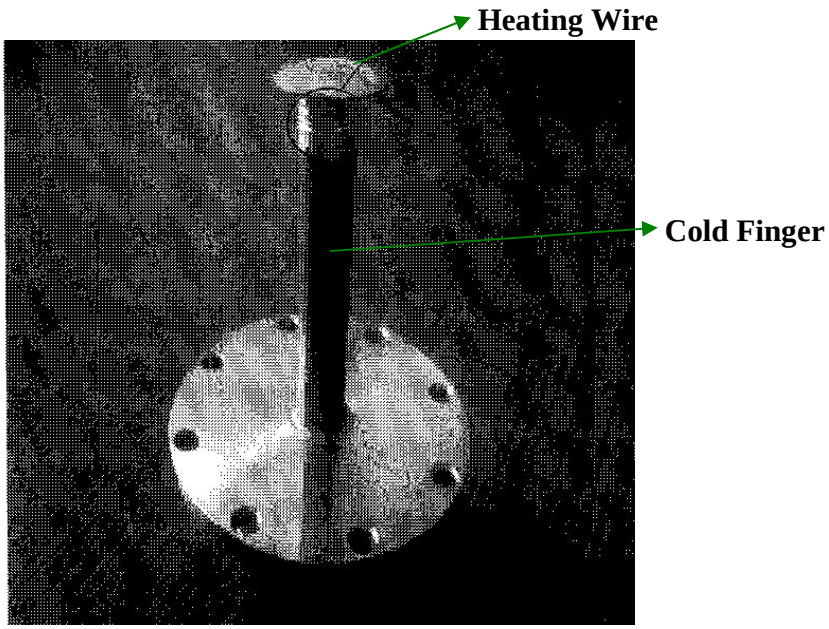

Fig (2.3): Photo of a cold finger and heating wire

This study measured the evaporation rate of liquid nitrogen to measure heat load of cryochamber by injecting liquid nitrogen at the end of low temperature area and generating heat load. The experiment was conducted at high vacuum level (less than 1.333×10^{-6} kPa) to eliminate convective heat transfer. As is expected, it was found that more the heat load supplied, higher was the evaporation rate of liquid nitrogen and vice

versa. The results further showed that heat transfer from outside in case of installation of radiation shield was 12.5% less than in the case when radiation shields were not used.

Outcome of Literature Survey

The prime of outcomes of the literature survey are summarized below,

1) The works by various researchers clearly outline the potential applications of the state of the art of IR sensors for BMD and space based applications.
2) One amongst various works is an experimental study carried out by Kang et.al [6] for transient cooling characteristics indicating that the cool down time alters significantly with changing inside pressure of infrared detector cryochamber beyond 1 torr.
3) Amongst a few works attempting thermal analysis by Kim et.al [7] steady cooling characteristics of a cryochamber have been investigated analytically in presence of radiation shields. The results showed that cryochamber vacuum should be maintained below 10^{-3} torr to limit heat inflow.
4) An experimental work by Kim et.al [8] investigating cryochamber operation under thermal load in presence of radiation shield concluded that the best operation range in terms of pressure is in the region below or around 10^{-3} torr.
5) It appears from the literature survey that existing works lack in terms of carrying out comprehensive thermal modeling of cryochamber detector assembly.
6) Even amongst the limited attempts that have been made with respect to thermal modeling most attempts have been using analytical models. It is well established that analytical modeling is limited to steady state scenario and transient cases cannot be investigated using these models.
7) Another aspect is the consideration of the radiative heat flux term in its original form, which is somewhat difficult to treat. Most works employ a pseudo convective term to model the radiation heat load which may lead to erroneous results at high operating temperatures.
8) Hence, in the present work a comprehensive numerical model is developed which is capable of analyzing both steady and transient operation scenarios considering radiation heat load in its original form.

Chapter 3
CRYOCHAMBER DESIGN ASPECTS

The design aspects of a cryochamber are governed by chosen area of application. The criticality is to provide at all times conditions suitable for storing liquefied cryogenic fluids or for achieving optimal operation of the device that they house. In case of cryochamber used for housing devices such as infra red detectors the design becomes even more critical. Since the design aspects such as, choice of material of the cryochamber, manner of electrical feedthrough, pressure of evacuation, glass to metal sealing etc are few of prime areas of concerns which influence the performance of the devices sealed in these cryochambers.

The present chapter discusses these design aspects of a cryochamber in sufficient detail to understand their role in achieving desired performance of the devices which in the present case is the infrared detectors.

3.1 Cryochambers or Dewars

The technical name for a vacuum bottle (commonly called a thermos bottle) is dewar (named after its inventor, Sir James Dewar). Several types of dewars are available, ranging from miniature glass packages less than an inch in diameter to enormous test chambers.

The cryogens generally boil away easily; the dewars are used to insulate them from higher temperatures. A carefully designed dewar reduces radiated, conducted, and convected heating as much as possible and a conscious effort is required to maintain the desired of degree thermal integrity.

These cryochambers / dewars can be classified as follows:

Storage dewars, for holding cryogenic fluids, such as, liquids of oxygen, nitrogen, air, argon and helium.

Laboratory test dewars for pre testing of any semiconductor device etc. in the laboratory itself and

Tactical dewars used in real warfare such as in missiles, battle tanks, etc.

The all glass chambers/dewars were used earlier for laboratory test purposes and were normally fed by liquid nitrogen only and were not found much useful for other purposes.

However, an infrared detector cryochamber/ dewar can be made up of all glass parts or all metal parts or by a glass-metal combination. Such tactical dewars used in warfare; need a compact and rugged design with easy portability (offering minimum heat load and physical weight).

3.2 Design Considerations for Cryochamber

The main data required for framing cryochamber specifications are as under:

1. Heat load of cryochamber
2. Operating temperature range
3. Material of cryochamber
4. Details of conductor leads
5. Bore and length of inner dewar
6. Outer diameter of dewar
7. Type of window, cold filter and cold shield
8. Degassing of dewar by baking
9. Vacuum sealing of dewar
10. Type of getters
11. Cool-down time and hold on time of cryochamber
12. Type of cryocooler
13. Mechanical integrity and ruggedness of cryochamber

3.2.1 Heat Load of Cryochamber

Normally following considerations are taken in estimating the heat load of cryochamber: [Refer fig. (3.1)]

i) Thermal conduction of cold finger (inner dewar tube)
ii) Thermal conduction due to conductor leads
iii) Gas conduction at low pressures and additional gas convection in case of pressure increase inside the cryochamber

iii) Radiation heat transfer on to cold finger (inner dewar tube)

iv) Radiative heat transfer through IR window on sensor surface

v) Thermal radiation by kovar parts of dewar

vi) Heat produced in sensor elements when the detector is operating

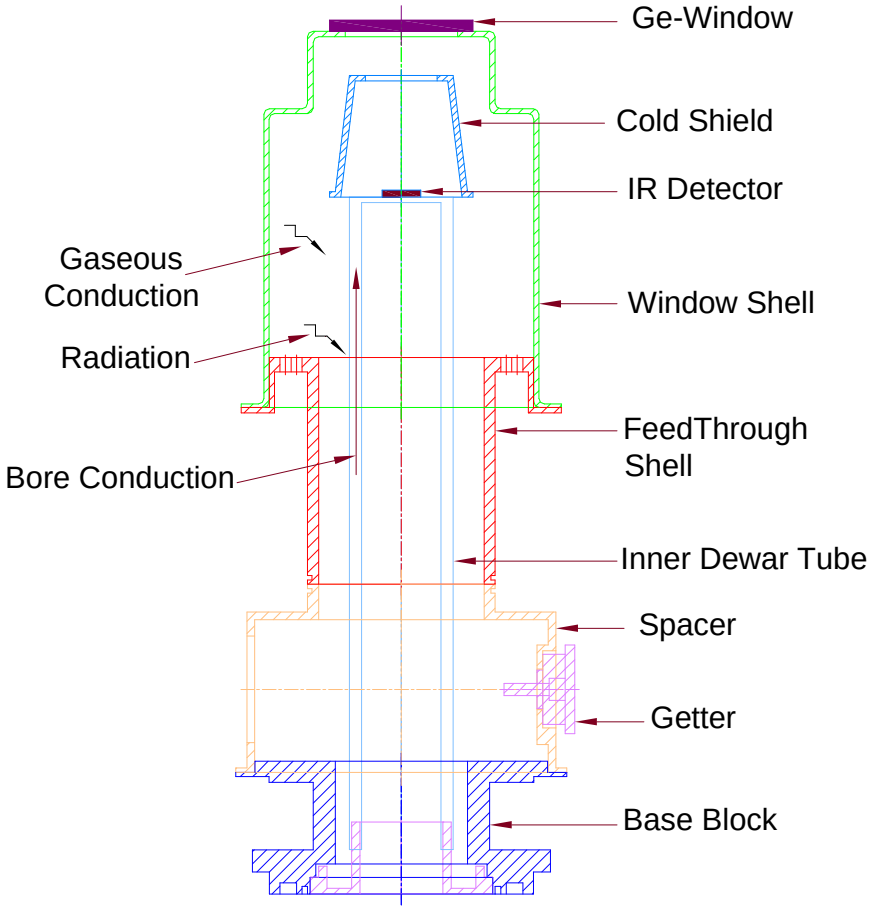

Fig (3.1): Schematic of a typical cryochamber and the mechanism of heat transfer

The heat leaks to dewar mainly arises due to solid conduction through the inner dewar tube and the metallic leads; thermal radiation from outer walls & Ge-Window at ambient temperature and finally by convection due to the residual gases present inside. In order to achieve a dewar with desired heat load, all the heat losses by conduction, convection and radiation have to be minimized. The solid conduction is reduced by using materials of low thermal conductivity, such as 'kovar matching glass', which has an

added advantage of its thermal expansion matching with kovar alloy, most widely used for glass to metal sealing. Similarly the lead conduction can be reduced by using thinnest possible (48 SWG) enameled copper wires or by thin flexi-circuits. Heat loss by radiation is minimized by using highly polished surfaces of low emissivity and finally the heat loss by convection is minimised by creating a high vacuum inside.

3.2.2 Operating temperature range

A cryochamber is normally supposed to operate between -40°C, say, in the region of snowcapped area to +70°C , say, in the deserts, the increased temperature may be due to the vehicle temperature in addition to the outside atmospheric temperature.

3.2.3 Material of Cryochamber

All metal cryochambers are normally made of stainless steel however for glass metal combination cryochamber normally, 'kovar' alloy and 'kovar-matching glass' is used as their coefficient of expansion or contraction matches closely. Kovar is an alloy of iron having following composition:

Ni = 29%; Co = 17%; Mn = 0.5%; Si = 0.2%;

C = 0.6%; and balance iron.

The average linear coefficient of thermal expansion (α) of kovar, in the range of 30 to 300°C, is = 4.86×10^{-6} cm/cm° C.

The kovar matching glass which is basically a borosilicate glass (corning 7052 or Schott 8250) has an average linear coefficient of thermal expansion (α'), in the temperature range of 0 to 300°C, is = 4.6×10^{-6} cm/cm° C.

This close matching of thermal co-efficient, makes kovar & kovar matching glass as an ideal combination for glass to metal seals for the fabrication for cryochambers as shown in fig. (3.2).

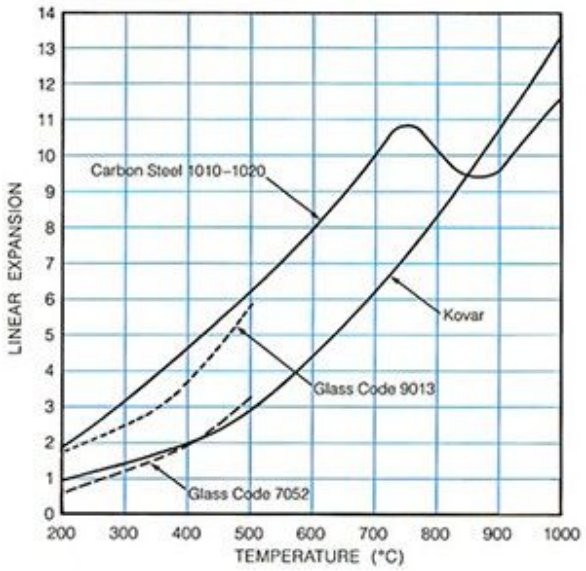

Fig (3.2): Curve showing close expansion relationship between Glass 9013 vs Carbon steel 1020, and Glass 7052 vs Kovar

Besides the excellent property of sealing to metals, glass has many other *advantages*, such as:

i) Good insulation properties,

ii) Low vapor pressure,

iii) Chemical inertness,

iv) Impermeability to gases, (except for H_2 & He, which are rare)

v) Workability to various shapes,

vi) Availability in many stock sizes

vii) Reasonable strength and cost

However, it has got some *disadvantages* also, such as:

i) Fragility to impact

ii) Poor mechanical strength in presence of strains,

iii) Poor thermal shock resistance

A notable property of kovar alloy is its comparatively low thermal conductivity which is 17 $Wm^{-1}K^{-1}$ at 30°C. It is about 23 times lower than that of copper at about the

same temperature, and matches closely to that of stainless steel. It is quite ductile and hence can easily be deep drawn.

3.2.4 Details of conductor leads

The type of connections used between the devices mounted inside, to the external feed-through has a direct bearing on the heat load of the dewar. Therefore, either very fine wires (enameled copper wires or phosphor bronze wires of about 2 mil dia (0.054mm) or 48 SWG (0.04mm) are used or gold tracks of about 2µm thickness (0.25mm wide) are used, running parallel to, or on the inner dewar surface itself. By using such fine geometries the heat load can be greatly reduced.

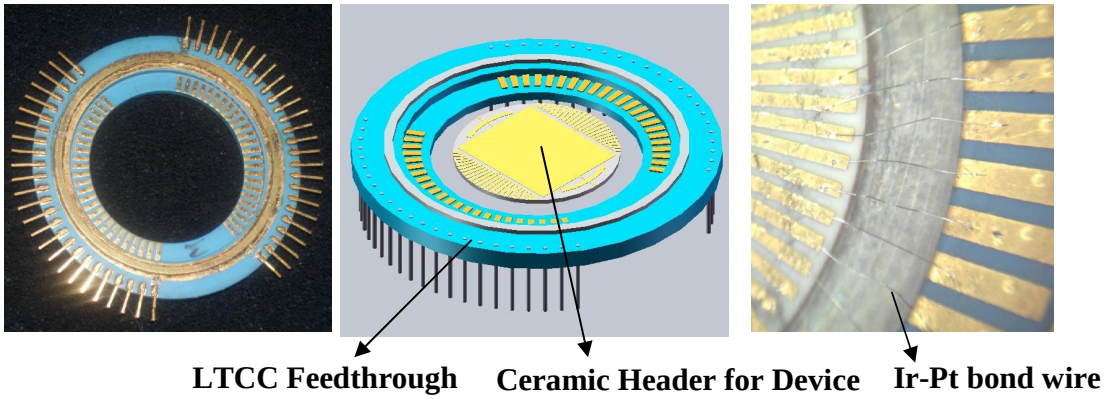

Fig (3.3): Wire Bonding of feedthrough to ceramic header with Ir-Pt wire

In some cases as shown in fig (3.3) a device placed on ceramic header is bonded to external LTCC (Low temperature cofired ceramic) feedthrough by 10% Ir-Pt wires, which have very low thermal conductivity as compared to aluminum and Phosphor bronze wires.

3.2.5 Bore and length of inner dewar

The method of cooling also to an extent influences the dimensions of dewar. In case Joule Thompson (JT) cooling is to be employed, there are very rigid tolerances requirement on the bore of inner dewar, for example, the bore has to be ±10µm and the

length of the tube should also not exceed by 3mm of the finned length of the cooler. However, in case of stirling cooler the tolerance on the bore are not so stringent.

3.2.6 Outer diameter of dewar

The outer diameter of the dewar is chosen on the basis of two criteria; one being the consideration of the space where it is to be mounted and secondly it is determined in order to provide sufficient vacuum insulation with respect to the inner dewar surface.

3.2.7 Type of window, cold filter and cold shield

The “window” is a radiation filter so as to allow only those radiations, which are in the range of the required wavelength to enter the cryochamber. For example, in case of IR devices normally the wavelength region of 8-14μm is acceptable. Thus, the window comprising of Germanium filters is employed which allows only wavelength in the range of 8 to 14μm to pass through. An anti-reflection coating is used to improve its efficiency so that the transmission may be increased to as high as 95%. The dimensions of window are selected based on the size of the dewar. The window should be strong enough to withstand vacuum pressure.

A cold filter, made of germanium, is also used over a cold shield to reduce the background further. A suitable (conical shaped) cold shield is required, which sits around the device as a radiation shield and gets cooled along with the device. The filter sitting over the cold shield also gets cooled (hence called cold-filter) which does better filtering due to its low temperature. The conical shaped cold shield also helps in providing a suitable “Field of View” for the detector.

3.2.8 Degassing of dewar by baking

The dewar should be degassed before it is finally sealed off from the pump. The degassing process is carried out on degassing setup consisting of turbo-molecular pump as shown in fig (3.4).

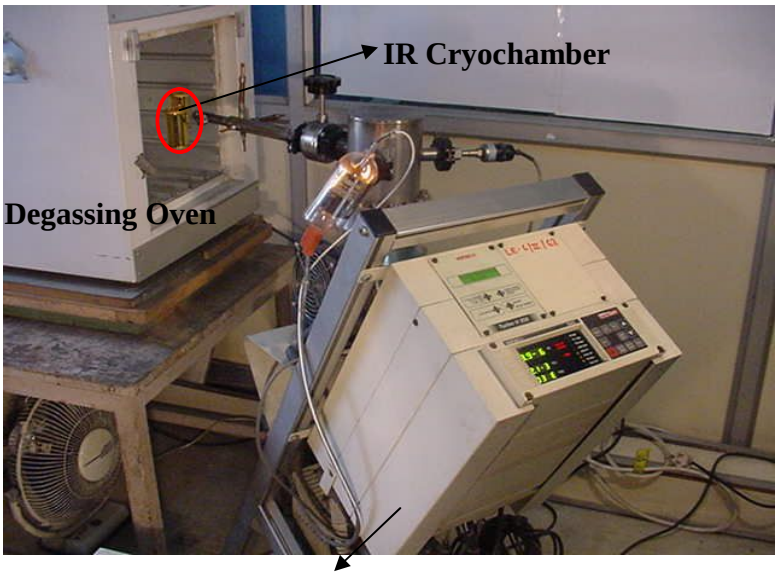

Fig (3.4): Cryochamber degassing station

The dewar parts normally adsorb gas molecules on their surfaces which have to be removed before sealing of their dewar. This gas evolution from the surfaces, called out-gassing, when exposed to the high vacuum, depends on the temperature of the surface, time of exposure to vacuum and on the characteristics of the particular gas or vapor. This process is sometimes called baking also as the temperature can be raised to as high as 400°C.

However, the temperature limit is given by practical considerations, for example, in case of dewars holding an IR device the temperature can not be raised beyond 65 to 70°C due to the limitation of the temperature tolerance of the device. A qualitative representation of the baking process is shown in fig (3.4). The length of the baking process varies from several hours to several days, which in case of the above mentioned dewars is about 7 to 8 days continuously without any break.

3.2.9 Vacuum sealing of dewar

The final sealing of the dewar is done in the vacuum of the order of 1 x 10^{-7} mbar after a prolonged degassing period of 7 to 8 days at the required temperature. If the dewar

outer shell as well as its evacuation tube is made of glass, then sealing is done with the help of a small flame torch which melts the glass and finally seals the dewar from the vacuum pump. However, if the outer shell of the dewar is metallic then normally OFHC (oxygen free high conductivity) copper tube is used for the evacuation purpose. The dewar is finally sealed by pinching-off process using a pinch-off tool. Both the methods are shown in fig (3.5). The low content of oxygen (less than 10ppm) in the OFHC copper tube helps in getting a perfect cold weld of the tube during pinching-off process and hence a high vacuum in the dewar can be retained.

a) Sealing by flame torch b) Sealing by cold welding

Fig (3.5): Vacuum sealing techniques for Cryochamber

3.2.10 Types of getters

A dewar whose inter-space is although evacuated, one cannot prevent the residual out-gassing from the inside material surfaces as the adsorbed and the penetrated gas molecules in the walls try to come out under high vacuum conditions. Therefore, in order to take care of this residual out-gassing, getters are used which are highly absorbing materials and act as auxiliary pumps, once the dewars are sealed, getters can reduce the pressure from 10^{-4} to 10^{-6} torr. When they are fired and can be fired from 10 to 12 times during the total shelf life of the tube, which can be extended beyond 10 years with the help of these getters.

There are basically two types of getters, viz. physio-sorption and chemisorption type. Normally the chemisorption type getters are used in dewars as their action is based on chemical combination with gas molecules and hence no restoration is required. These non-evaporable chemisorption type getters are generally made up of Zr-V-Fe and have following advantages:

a) Low activation temperature,
b) They can be reactivated several times to present fresh surfaces and
c) They have remarkable gettering action even at room temperature.

The typical getters in dewars and their action is shown in fig (3.6).

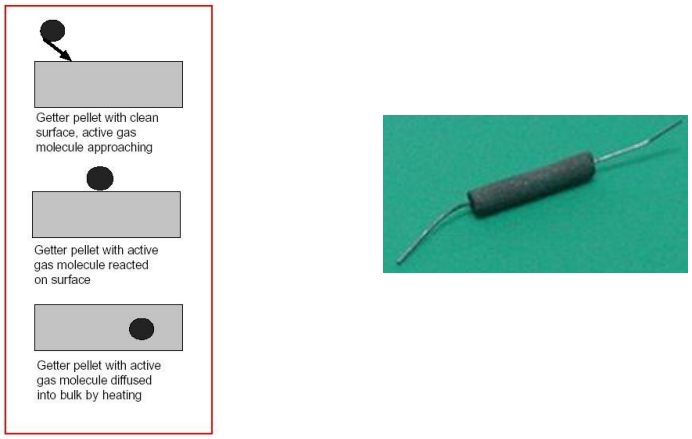

a) Getter action b) Non-evaporable chemisorption getter

Fig (3.6): Typical getter action along with types of getter used in cryochambers

3.2.11 Cool down time and Hold on time of cryochamber

The cool down time of a dewar can be defined as the time taken in cooling the device from room temperature to the required cold temperature of operation which in our case is 77 K, i.e., the liquefaction temperature of nitrogen gas. Depending upon the capacity of the cooler and the heat load of the dewar, the typical values of cool down time of 2 to 3 minutes can be achieved. Similarly, the hold on time of dewar can be defined as the time for which the device remains stable at the operating cold temperature of 77 K after the high pressure gas is cut off to the JT cooler or power input is switched off to

Stirling cooler. The typical values of about 30 seconds to 1 minute can be achieved depending upon the thermal capacity of the dewar.

3.2.12 Type of cryocooler

Cryocooler is required to obtain requisite cryo- temperature inside cryochambers. These generally incorporate the same kind of insulating techniques as those used for dewars, and require the same precautions. Refrigerators are of two principal types: closed-cycle refrigerators, which recycle the same fluid (often helium) over and over; and open-cycle refrigerators, which draw from a high pressure tank of gas, with the gas vented to the atmosphere after it performs its cooling. Prior to discussing the various kinds of cryocooler, the basic characteristics of cryocooler are discussed foremost.

a) Characteristics and requirement of cryocooler

The cooling capacities required range from fractions of a watt (milli-watts) to as much as 10 W at temperatures extending from a minimum of 1K or less to those well above the limit of the cryogenic range (arbitrarily defined as 120 K).

Cryocoolers are often rated by their available refrigeration capacity measured in watts. In order to be meaningful, however, it is necessary to specify not only the refrigeration capacity but also the temperature. Since the refrigeration capacity for a cryo-cooler having a capacity of 1 W at 80 K (liquid nitrogen temperature) is very much different at say 1 K. Another important parameter is the power input or work required to achieve the desired refrigeration capacity.

The coefficient of performance of a refrigerator is defined as the ratio:

COP = refrigeration capacity / power input or

COP = heat lifted / work done

The ideal coefficient of performance is the carnot value:

$$COP_{carnot} = \frac{T_R}{(T_C - T_R)}$$

where, T_R is the minimum cycle temperature (usually the refrigeration temperature) and T_C is the maximum cycle temperature (generally the atmospheric temperature).

The ratio of the actual coefficient of performance to the carnot coefficient of performance is called the efficiency (η). It is a useful measure of the way an actual machine measures up to the thermodynamic ideal machine. Thus:

$$\eta = \frac{COP_{actual}}{COP_{carnot}} = \left(\text{Re } f.capacity / Powerinput\right) \Big/ \left(T_R / T_C - T_R\right)$$

The efficiency of currently available cryocoolers ranges from a minimum of less than 1 % to a maximum of nearly 50 %.

The miniature cryocoolers used for electronic applications have the lowest efficiencies. This is because nearly all the refrigeration generated is consumed in cooling, and maintaining cold, the low temperature region of the machine itself. The surplus or useful refrigeration, the available refrigeration from these units, is very small (fractions of a watt). Those applications that impose a larger refrigeration load use bigger refrigerators that tend to be more efficient.

The significant parameters for cryocoolers include the total mass and volume of the system and sometimes the mass and volume of the cold region. The latter is of particular importance in infrared missile guidance systems with cooled detectors and associated optical / electronic systems mounted in swiveling gimbals. A low mass and volume are necessary to facilitate a fast response with low inertia forces.

The cool-down time, the period necessary for the machine to achieve stable operation at the design condition following start-up is important in many applications of miniature systems, particularly those that are weapons related. The combination of a quick cool down and a slow warm-up is a particularly challenging requirement involving mutually opposed high and low thermal masses. Cool down is sometimes accelerated by operating at start-up with a high pressure or speed and later reverting to the normal operating mode.

Mechanical vibration and electromagnetic emission in the cold region are often important characteristics of cryocoolers. Some applications require virtually the total elimination of any mechanical or electromagnetic noise.

This is best approached by:

i) Physical separation of the cold region and the compressor unit where large power input and heat transfer take place;

ii) Elimination of moving parts in the cold region;

iii) The use of plastic, ceramic, or other non-magnetic parts in cold region.

Operating life is another important characteristic often quoted as the mean time before failure (M.T.B.F.) or the mean time before maintenance (M.T.B.M.). This is generally taken to imply the average time of operation before failure (or maintenance) of a number of identical cryocoolers operating under similar conditions.

b) Cryocoolers in Infrared detector cryochamber

Type of the cooler is decided based on the application. For missile application, where the system is on board and the available time for cooling is short, a Joule Thomson (JT) mini-cooler is used but if the dewar is required for ground based applications such as for the thermal sight of either a battle tank or a missile carrier, and the usage is also for a longer duration, a Stirling cooler is more suitable.

Basically these are two types of cryocoolers, which are used for cooling in infrared detector cryochambers.

i) JT Minicooler : Joule Thomson Cryocoolers are based on J-T effect, named after the two British Scientists, J.P. Joule and William Thomson (later Lord Kelvin), who discovered this very simple but most useful principle in 1850 at Manchester, England. The principle says 'If a gas is expanded from high pressure to low pressure through an orifice at constant enthalpy, it will experience a temperature drop.' The effect of change in temperature for an isenthalpic change in pressure is represented by Joule-Thomson coefficient $\boldsymbol{\mu}_{JT}$ defined by

$$\boldsymbol{\mu}_{JT} = (\partial T / \partial P)_h$$

For a real gas, $\boldsymbol{\mu}_{JT}$ can be + ve or – ve depending upon the fluid temperature before expansion.

For an ideal gas, $\boldsymbol{\mu}_{JT}$ is zero. Fig (3.7) shows a plot between temperature (T) and pressure (P) for various enthalpies i.e. for real gas. In order to obtain cooling, we should operate in the region located in the left of inversion curve.

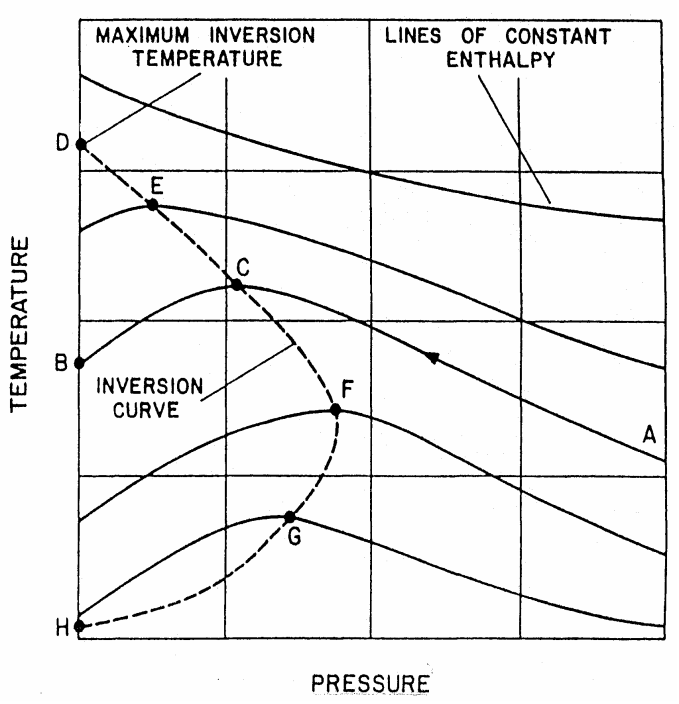

Fig 3.7: T and P plot for various enthalpies showing inversion curve

The maximum inversion temperature of various gases is as indicated in the table below,

Gas	Max. Inversion Temperature (K)
Above ambient	
Carbon dioxide	1500
Oxygen	760
Argon	722
Nitrogen	623
Air	602
Below ambient	
Neon	250
Hydrogen	202
Helium	40

Table (3.1): Maximum inversion temperature of various gases

Fig (3.8): Typical hardware of JT cooler

Normally, high pressure (3000psi) nitrogen gas below its inversion temperature (623K) is expanded through an orifice of about 50µm, causing a drop in temperature. The expanded gas cools the incoming gas through a heat exchanger and regenerative cooling occurs until the liquid is formed. In order to achieve maximum efficiency from this heat exchanger, the fit of the JT cooler to cryochamber need to be in a very close tolerance of about ± 10µm. The JT cooling system basically requires a high pressure gas storage bottle, solenoid gas release valve, gas cleaner, high pressure fittings and gas line, a mini-cooler head and the detector dewar as shown in the fig. (3.8).

The merits of JT cooler are given below,

i) Instant cooling
ii) Better temperature stability
iii) Small weight & bulk
iv) Simple and silent operation
v) No requirement of electrical power
vi) Absence of moving parts
vii) Reliable and rugged

The demerits of JT cooler are given below,

i) Higher operating pressure
ii) Limited refrigeration capacity

iii) Operating time is a function of gas reservoir capacity

iv) Prone to blockage

v) Filtration requirements are high

vi) Logistics due to booster, gas supply and storage requirements

ii) Stirling cooler : This cooler works like a refrigerator in a closed cycle, when power input is given to it. This cooler is available both in integral version (when compressor and cold finger are in one piece) as well as in split version (where compressor and cold finger are connected by flexible tube. So, depending upon the design of this cooler, the dewar is designed accordingly.

Basically the stirling cooler works on the stirling cycle which is made up of two isotherms and two isochoric regenerative processes as shown in fig. (3.9).

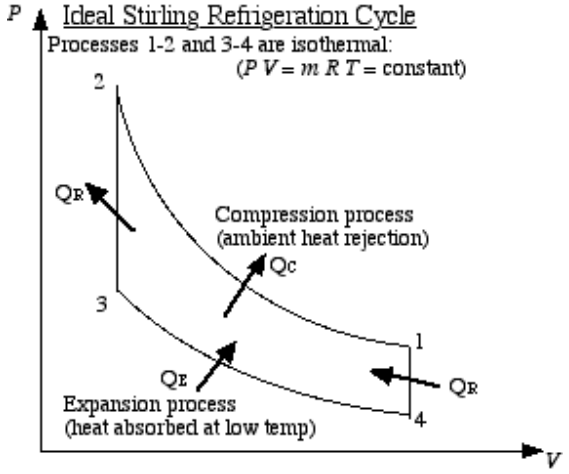

Fig (3.9) Thermodynamic cycle of a stirling cooler

In the process 1-2 of isothermal compression, the working fluid (helium) is compressed but its temperature is maintained constant as heat is rejected to the surroundings. In process 2-3 of isochoric heat transfer, the working fluid is transferred through a porous metallic matrix of regenerator; hence it experiences a decrease in temperature from T_c to T_e as heat Q_R is transferred from working fluid to the regenerator.

In the process 3-4 of isothermal expansion the temperature is maintained constant as heat Q_E is extracted from the refrigerated space. Finally, in the process 4-1 of isochoric

heat transfer, the working fluid experience an increase in temperature from T_e toT_c as heat Q_E, which was stored in process 2-3, is released from the regenerator matrix to the working fluid. This is how the cycle repeats and the stirling cooler produces cooling.

When compared to JT mini-cooler, the stirling cooler does not need any continuous high-pressure gas supply and hence fewer accessories are required. All that is needed is power supply and then it can run for hours together, which makes it useful for the application of night vision in the battle tanks, etc.

iii) Alternative Cooling Methods

Radiation coolers have been extensively used in space applications. They face the sky (which in space is very cold) and radiate energy away into space. They require no operation fluid and have no moving parts except the mechanisms required to keep them pointing away from the sun.

Thermoelectric (TE) coolers provide cooling by forcing current through a junction of dissimilar metals. These coolers are small, simple, and reliable, generate no audible noise, and operate in any orientation. Their primary disadvantages are the relatively large amount of electrical power required to achieve a given cooling level, and the limited temperatures that can be reached.

3.2.13 Mechanical integrity and ruggedness of cryochamber

To reduce the conducted heat load, the mechanical supports are made as small as possible and special materials are used. The following special treatment is necessary:

- Handle the dewars gently; they are often fragile.
- Any wiring from the cold stage should be handled carefully and changed only after a thermal analysis.
- Special surface preparation is essential to avoid radiated heat leaks

Depending upon the application of dewar, its ruggedness is decided and accordingly the dewar is designed. The necessary ruggedness of the dewar can be pre-tested, by subjecting the dewar to number of environmental tests as described below:

i) *Random vibration testing*: Typical values are about $0.02g^2$ / Hz between 20 to 2000Hz for about 5 minutes at X, Y and Z axes.

ii) *Acceleration test*: Typical values are about 10-15g longitudinally and at 10-12g laterally for about 10 seconds each.

iii) *Bump test*: At the rate of 100bumps/minute with bump height of about 1 inch.

iv) *Shock test*: At 40 to 50g in 10milliseconds.

Before each environmental test the dewar is subjected to radiography tests and studied for any visual damage. After test is over, once again radiography is repeated and compared with the radiography results prior to performing integrity tests. If no damage is observed than the dewar is declared for application.

Chapter 4
NUMERICAL SIMULATION

The investigation of cooling characteristic of an infrared detector cryochamber is actually a relatively complex heat transfer problem. This occurs primarily because of the kind of heat transfer processes involved in the analysis.

In a cryochamber, conduction and radiation occur simultaneously and both steady and transient responses are important. Due to these seemingly complex heat transfer processes, very few modeling efforts have been undertaken till date.

The present chapter focuses on the modeling of heat transfer processes, and the analysis of variation of parameters on cooling performance of cryochamber in both steady and transient operation modes. The possibility of use of analytical methods is limited only to steady state analysis and cannot be employed for transient thermal analysis. It is because it involves use of error function which is highly computationally intensive, therefore, a generalized numerical approach has been used for both steady and transient thermal analysis.

4.1 Domain configuration

The thermal modeling for a generalized cryochamber domain has been carried out, the typical configuration of which is as shown in fig (4.1) below. Basically, the cryochamber has the following components viz., i) consists of a vacuum vessel (outer cylinder), ii) a cold well (inner axisymmetric thin walled structure), and iii) a feedthrough unit, iv) IR detector is located on the top of the cold well, v) IR window i.e. the roof of the cylinder through which the detector receives the signal.

The space between the vacuum vessel and the cold well is maintained under vacuum to minimize heat loss. The cold well shape is mostly cylindrical and the cooling is executed by an external cooler, which may be based on various refrigeration schemes such as; Stirling, Joule – Thomson, already been discussed in Chapter -3, section – 3.2.12 .

The vacuum vessel is made of stainless steel material, whereas the cold finger is a thin cylindrical vessel made of glass or steel. It is evident that the thickness in case of glass will be greater than in steel on account of its mechanical integrity. The base is again made of stainless steel.

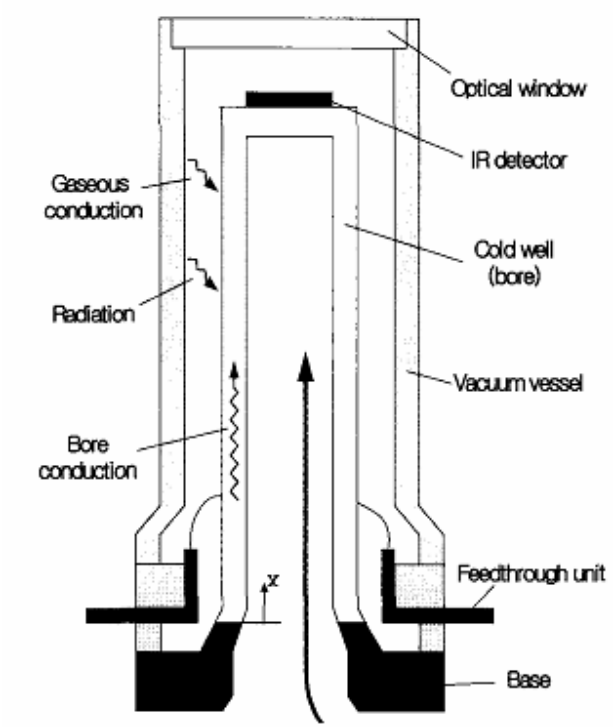

Fig (4.1): Schematic a typical cryochamber and modes of heat transfer

4.2 Modes of heat transfer

In order to correctly solve the problem the foremost objective is to ascertain the possible modes of heat transfer. Simultaneously, it is also essential to identify those possible modes of heat transfer whose contribution is negligible. In the final analysis these latter modes of heat transfer will be neglected greatly simplifying the problem to obtain realistic results. The possible modes of heat transfer in the present case are;

i) Heat conducted from the base to the top of the cold well along the thin wall

ii) Radiative heat transfer occurs between the inner surface of the vacuum vessel and outer surface of the cold well.

iii) Natural convection on to the cold well

iv) Although, domain is under vacuum, however, the remaining gas may participate in heat transfer on account of gaseous conduction.

v) In steady state operation, another additional heat load is heat generated by the detector on biasing. The cryocooler has to be designed accordingly.

Here, it is pertinent to mention that heat load due to natural convection, designated as (iii) may be neglected. This mainly because of the small dimensions of the domain, natural convection hardly makes a significant contribution. Further, if one were to determine the Nusselt number based on gap spacing for the given annular interior space (solved as a vertical large aspect ratio enclosure) for any applicable configuration, it would mostly turn out be unity [9].

Assumption for analysis

i) Heat transfer due to convection may be neglected.

ii) Since the cold well is a thin cylinder (typical thicknesses close to 1mm), the conduction may be considered to be one dimensional i.e. along the axis. If one were to calculate the Biot number, it would turn out be of the order of 0.02, indicating that transverse gradients are negligible.

iii) The cryocooler inserted into the bore has the same temperature distribution as the cold well, thus neglecting heat transfer analysis at the internal surface of the cold well.

iv) The thermal contact resistance between the metal (stainless steel) base and the glass bore since the glass is typically fused to be bond to the base. Therefore, 'T_b' is the same as the temperature of the metal base, which is identical to the ambient temperature 'T_∞'.

v) At the other end detector array is bonded to the glass bore by an epoxy and it is assumed the temperature of the end of glass bore is same as the detector (T_d).

vi) The shape factor, which in the present case is the fraction of energy leaving the vacuum vessel and intercepted by the cold well, for radiation heat transfer is unity.

4.3 Thermal modeling

The thermal modeling of the cryochamber has been carried out for both steady state as well as transient conditions. The formulation for steady state case is discussed below.

4.3.1 Formulation for steady state heat transfer

The basic energy balance for an elemental volume of the coldwell in case of steady state heat transfer is shown in fig (4.2).

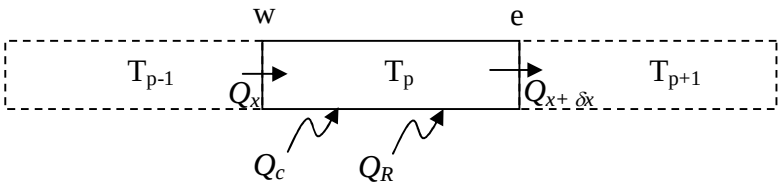

Fig (4.2): Heat transfer in an elemental volume of coldwell

Hence, this can be mathematically represented as,

$$Q_w + Q_c + Q_R = Q_e \qquad \textbf{(4.1)}$$

The terms *'Q_w'* and *'Q_e'* represent the heat being conducted into the finite volume and away from it and can be expressed using the Fourier's law.

'Q_c' represents the term because of *gaseous conduction* and is expressed as function of heat transfer coefficient, temperature difference and the circumfrential area of the finite volume under consideration.

'Q_R' represents the radiative heat transfer which is mathematically expressed by means of the Stefan Boltzmann law.

Thus mathematically, Eq. (4.1) may be transformed as in Eq. (4.2)

$$-kA(dT/dx) + P\delta x h(T_a - T_p) + P\delta x \sigma\varepsilon(T_a^4 - T_p{}^4) = -kA(dT/dx) + \frac{d}{dx}(-kA\frac{dT}{dx})\delta x \qquad \textbf{(4.2)}$$

Further, simplifying the equation we get,

$$kA\frac{d^2T}{dx^2} + Ph(T_a - T_p) + \sigma.P\varepsilon(T_a^4 - T_p{}^4) = 0 \qquad \textbf{(4.3)}$$

Eq. (4.3) can further be modified as,

$$\frac{d^2T}{dx^2} + \frac{Ph}{kA}(T_a - T_p) + \frac{\sigma.P.\varepsilon}{kA}(T_a^4 - T_p{}^4) = 0 \qquad \textbf{(4.4)}$$

In order to solve the problem numerically, Eq. (4.4) is to be integrated over the finite volume from control surface *w'* to control surface *'e'*. Thus, Eq. (4.4) may be expressed as,

$$\int_w^e \frac{d^2T}{dx^2}dx + \int_w^e \frac{Ph}{kA}(T_a - T_p)dx + \int_w^e \frac{\sigma.P\varepsilon}{kA}(T_a^4 - T_p{}^4)dx = 0 \qquad \textbf{(4.5)}$$

Term (I) Term (II) Term (III)

Term (I) and term (II) can be expressed for discretization quite easily. Hence, Eq. (4.5) may be written as,

$$\left(\left.\frac{dT}{dx}\right|_e - \left.\frac{dT}{dx}\right|_w\right) + \frac{Ph}{kA}(T_a - T_P)\Delta x + \frac{\sigma.P\varepsilon}{kA}T_a^4.\Delta x - \int_w^e \frac{\sigma.P}{kA}\varepsilon T^4 dx = 0 \qquad \textbf{(4.6)}$$

However, a part of the term (III) is non linear term as clearly evident in Eq. (4.6) with finite volume representative temperature appearing as a power of '4'. Hence, it needs to be linearized. The linearization procedure adopted is as suggested by Patankar et. al [10]. The last term of Eq. (4.6) i.e. $\int_w^e \frac{\sigma.P}{kA}\varepsilon T^4 dx$ may be treated as a source term (S) and expressed as,

$$S = S_c + S_p T_p = S^* + \left(\frac{dS}{dT}\right)^* \left(T - T^*\right) \qquad \textbf{(4.7)}$$

Here '*' values represent previous iteration values of the variable being sought, which in this case is *'T_p'*. As will evident later when we discuss the operating algorithm, the solution of the equation (4.5) would require iteration for non – linearity. The terms *'S_c'* and *'S_p'* turn out to be,

$$S_c = -3.\frac{\sigma.P}{kA}.\varepsilon.T_p^{*4}$$

$$S_p = 4\frac{\sigma.P}{kA}.\varepsilon.T_p^{*}$$

Thus, Eq. (4.6) on discretization may be written as,

$$\left[\frac{T_{P+1} - 2T_P + T_{P-1}}{\Delta x}\right] + \frac{Ph}{kA}.T_a.\Delta x - \frac{Ph}{kA}T_P.\Delta x + \frac{\sigma.P}{kA}.\varepsilon.T_a^4.\Delta x - \frac{\sigma.P.\varepsilon}{kA}\Delta x[-3T_P^{*4} + 4T_P^{*3}.T_P] = 0 \quad \textbf{(4.8)}$$

Thus, rearranging Eq. (4.9) in the generalized form representing the discretization equation we have,

$$a_P T_P = a_e T_e + a_w T_w + b \quad \textbf{(4.9)}$$

Where,

$$a_P = \frac{2}{(\Delta x)^2} + \frac{Ph}{kA} + \frac{\sigma.P}{kA}\varepsilon.4T_P^{*3}$$

$$a_e = 1/(\Delta x)^2$$

$$a_w = 1/(\Delta x)^2$$

$$b = \frac{\sigma.P}{kA}\varepsilon.3.T_P^{*4} + \frac{Ph}{kA}T_a + \frac{\sigma.P}{kA}\varepsilon.T_a^{*4}$$

Boundary conditions

i) 'T_b' is the same as the temperature of the metal base, which is identical to the ambient temperature 'T_∞' i.e. 300 K.

ii) The end of glass bore temperature is the one optimal for IR detector operation i.e. 'T_d' which is 77 K in the present case.

Thus the boundary conditions are case of Drichlet boundary with fixed temperatures being specified at both the boundaries.

Working algorithm

The basic algorithm for solution of steady state cryochamber heat transfer problem is as under;

i) Define the input conditions; material properties, boundary conditions and geometry of the domain to be evaluated.
ii) Define the number of control volumes
iii) Discretize the equation and calculate the coefficient a_p, a_w , a_e , b from the input conditions for each control volume.
iv) Specify the applicable boundary conditions
v) Solve the equations using standard Tridiagonal Matrix algorithm (TDMA) to generate the temperature field along the length of the cold well.
vi) Iterate for non linearity of the equation till convergence criterion of 1e-3 is met.

The developed program in Matlab is attached in Appendix –A.

4.3.2 Formulation for transient heat transfer

In case of infrared detector analysis, transient heat transfer analysis is even more critical as it is often essential that ready should be ready for work within a short span of time, especially when one envisages defense applications. The time the detector takes for the temperature to reach 77 K, its typical operating temperature from ambient temperature is termed as the cool down time. It is the foremost measure of the transient performance of the detector cooling system. The energy balance in the cold well, from one – dimensional unsteady state conduction and surface heat flux is given by the following equation.

$$\frac{1}{\alpha}\frac{\partial T}{\partial t} = \frac{d^2T}{dx^2} + \frac{m^2}{\rho.C}(T_a - T_p) \qquad \textbf{(4.10)}$$

Where,

$$m = \frac{hP}{kA}$$

In this case, the term *'h'* incorporates both the effects of gas conduction due to outgassing and radiation heat transfer. The other generalized way of expressing the heat

balance is given in Eq. (4.11) in which the gas conduction terms and radiation terms are dealt with separately and *'h'* represents only gas conduction heat transfer coefficient.

$$\frac{\partial T}{\partial t} = \alpha \frac{d^2T}{dx^2} + m^2\alpha(T_a - T_p) + r^2\alpha\left(T_a^4 - T_p^4\right) \qquad \textbf{(4.11)}$$

$$r^2 = \frac{P\sigma\varepsilon}{kA}$$

On linearization in a manner slightly different from Eq, (4.7), with $S_p=0$, the entire weight of the radiation term is modeled as a source term. It is done mainly to reduce the computation complexity. Hence, Eq. (4.11) on applying the above linearization becomes,

$$\frac{\partial T}{\partial t} = \alpha \frac{d^2T}{dx^2} + m^2\alpha(T_a - T_p) + r^2\alpha(T_a^4 - T^{*4}_p) \qquad \textbf{(4.12)}$$

In order to carry out transient analysis, the above equation may be discretized using finite volume method by integrating over both space (Δx) as well as time step (Δt). The discretized equation for the case of explicit formulation is given in Eq. (4.13).

$$T_p^{n+1} = T_p^n + \frac{\alpha\Delta t}{\Delta x^2}\left[\frac{T_{p+1}^n - 2T_p^n + T_{p-1}^n}{(\Delta x)^2}\right] + m^2\alpha\left(T_a - T_p^n\right)\Delta t + r^2\alpha(T_a^4 - T^{*4}_p)\Delta t \qquad \textbf{(4.13)}$$

Boundary conditions

It is considered that the cold well detector is at 'T_a' and begins to cool as the cooler operates at the cold tip. The base temperature is considered to be constant at 'T_a' at all time. Therefore, the initial condition is

At, $t=0$, $T = T_a$ for $\forall$ 'x'

The boundary condition for each time step calculation is,

i) $T = T_a$, at $x = 0$ at $\forall$ 't'

i.e. a Drichlet boundary condition

ii) The boundary condition at the detector size is slightly more complicated. One has to assume that the cryocooler refrigeration capacity is a linear function of the existing temperature, therefore

$$Q_c = aT(t, x = L) + b \qquad \textbf{(4.19)}$$

Thus, the energy balance at the tip grid is written as follows, which serves as the Neumann boundary condition.

$$\frac{\partial T}{\partial t} = \alpha \left.\frac{\partial T}{\partial x}\right|_{x=L} + m^2\alpha(T_a - T_p)\Delta x + r^2\alpha(T_a^4 - T^{*4}{}_p)\Delta x - (aT + b) \qquad \textbf{(4.20)}$$

Working algorithm

The basic algorithm for solution of transient cryochamber heat transfer problem is as under;

i) Define the input conditions; material properties, boundary conditions and geometry of the domain to be evaluated.
ii) Define the number of control volumes
iii) Establish the governing equation considering all heat transfer processes.
iv) Discretize the equation to be solved in an explicit formulation.
v) Iterate for non linearity of the equation till convergence criterion of 1e-3 is met at each time step.

The developed program in Matlab is attached in Appendix –B.

a. Variation in gas conduction coefficient (h)

Since cryochambers operate in very low pressure regime (from 10^{-5} to 1 torr), the mean free path (λ) cannot be neglected vis –a viz the minimum characteristic dimension (l). This requires consideration of heat transfer in rarefied gas whose theory is quite well known [11, 12]. The degree of rarefaction is defined in terms of Knudsen number ($Kn = \lambda/l$) determines the heat transfer regimes as follows:

i) Free molecular regime for $Kn > 10$
ii) Transition for $0.1 < Kn < 10$
iii) Temperature jump or slip regime $0.01 < Kn < 0.1$
iv) Continuum $Kn < 0.01$

A more practical parameter which may be the basis for categorization of heat transfer regimes is gas pressure. In order to do that, first a quantity 'P_{fm}' is defined as pressure below which free molecular conduction is pre-dominant and also gas pressure in the

range of 1 torr are considered to be representing continuum regime. Further, considering the ratio of heat fluxes for slip and continuum fluxes, criterion for regimes is defined as,

$$h = 1.48P \text{ for } P < P_{fm} \quad \textbf{(4.21)}$$

where, $P_{fm} = \dfrac{k_B T_m}{10\sqrt{2} d^2 l}$

P_{fm} = 4×10^{-4} torr

k_B = Boltzmann constant (=1.38054×10^{-23} JK^{-1})

T_m = Average temperature between minimum and maximum temperature

d = Molecular diameter of air (= 0.37)

$$h = \frac{1.48P}{1 + 0.34P} \quad \text{for } P_{fm} < P < 1 \text{ torr} \quad \textbf{(4.22)}$$

$$h = 4.35 \quad \text{for } P > 1 \text{ torr} \quad \textbf{(4.23)}$$

4.4 Numerical Results

The present section is devoted to the presentation of parametric results of thermal modeling of cryochamber. The results for steady state analysis are taken up foremost.

4.4.1 Numerical Results: Steady state

Considering, a typical case of glass cryochamber having the material and transport properties as given in table (4.1) below, the temperature profile along the length was determined.

In order to check the efficacy of the numerical model developed the first task is to perform the grid convergence check. The grid convergence check is carried out by varying the no. of grids. In the present case the above problem has been solved employing 24 grids, 48 grids and 96 grids, and overlapping temperature profiles have been obtained, as shown in fig (4.3).

Hollow glass cryochamber (Case-I)	
Outer diameter	9 mm
Inner diameter	7 mm
Length	48mm
Density	2640 kgm^{-3}
Gas conduction coefficient	0.632 $Wm^{-2}K^{-1}$(≡ 0.5 Pa or 3.8 x 10^{-3} torr)
Thermal conductivity	0.8 $Wm^{-1}K^{-1}$
Specific heat	800 $Jkg^{-1}K^{-1}$
Emissivity	0.02
Base Temperature	300 K
Detector temperature	77 K

Table (4.1): Dimension and properties of glass cryochamber

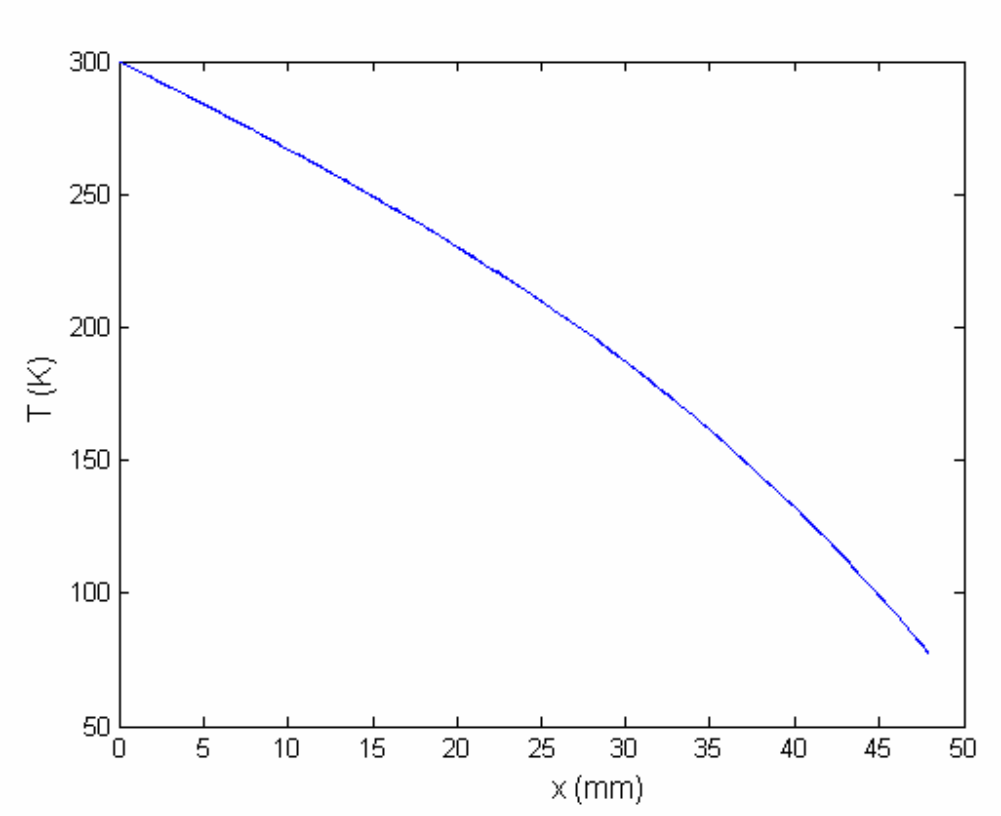

Fig (4.3): Grid convergence check for numerical model of cryochamber

Three set of grids, 24, 48 and 96 have been used

After, establishing the effectiveness of the model a parametric analysis for the same geometry is done by varying the gas conduction coefficient *(h)*. The gas conduction coefficient is essentially a function of pressure inside the cryochamber and is found to increase with increase in pressure. The effect on temperature profile for various gas conduction coefficient has been shown in fig (4.4).

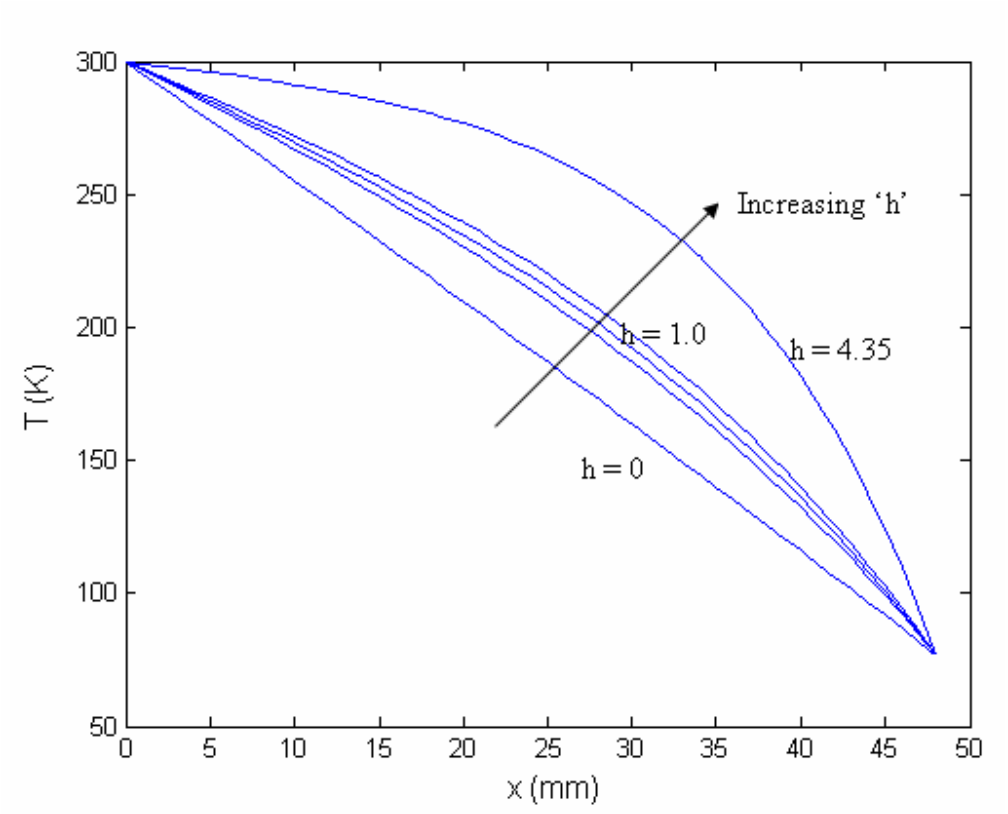

Fig (4.4): Length profile of temperature for various gas conduction coefficients *h* = 0, 0.632, 0.8, 1.0, 4.35 have been studied

Another, parameter that may vary owing to the extent of polishing of the cryochamber surface is the emissivity *(ε)*. Hence, the temperature profile has been generated by varying the emissivity and is shown in fig (4.5).

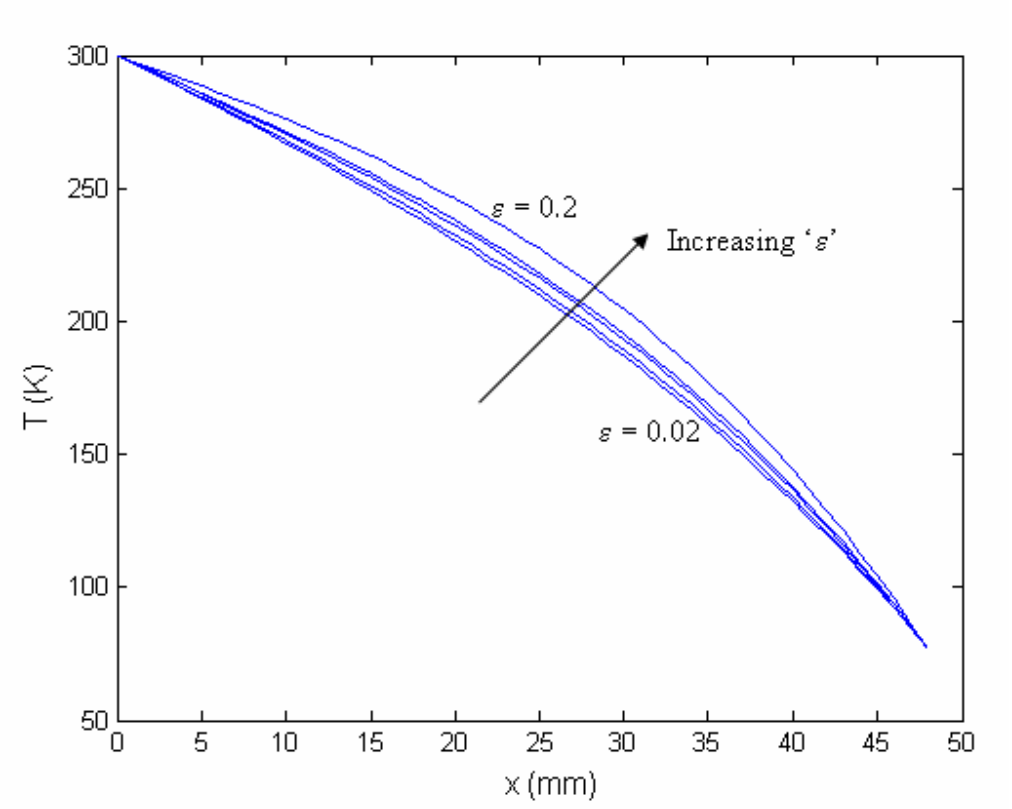

Fig (4.5): Length profile of temperature for various emissivities

ε = 0.02, 0.04, 0.08, 0.1, 0.2 have been studied

The Case-I corresponds to the geometry used by Kim et.al. [5] and the numerical results are in line with the analytically expected results. The Case-II solved is for our cryochamber geometry and stated values of thermal conductivity and gas conduction coefficient as given in table (4.2) below while all remaining transport and material properties remain same as in table (4.1).

Glass cryochamber (our experiments) (Case-II)	
Outer diameter	9.4 mm
Inner diameter	7.2 mm
Length	42 mm
Thermal conductivity	1.2 $Wm^{-1}K^{-1}$
Gas conduction coefficient	1.0 $Wm^{-2}K^{-1}$($\equiv$ 0.9 Pa or 6.84 x 10^{-3} torr)

Table (4.2): Dimensional details of our glass cryochamber

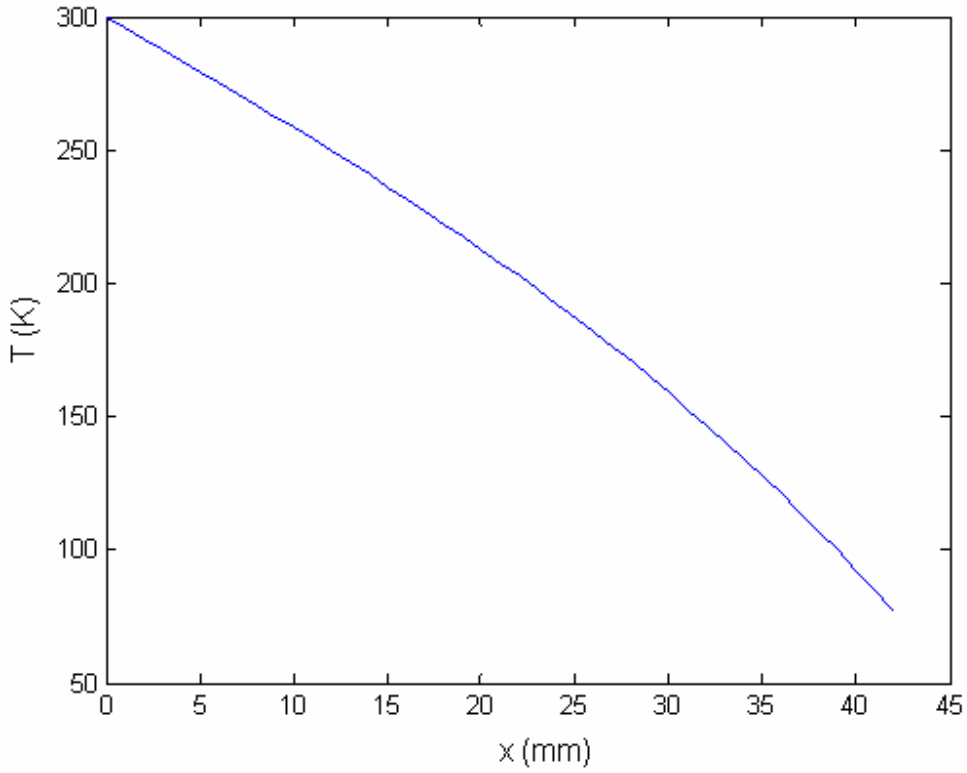

Fig (4.6): Length profile of temperature for various gas conduction coefficients *h* = 1.0 have been studied

The results, of the length profile of temperature shown in fig (4.6) as expected are qualitatively similar to those obtained for Case–I for the considered gas conduction coefficient of unity.

Another case analyzed was for a hollow metal cryochamber (Case–III), the typical material and transport properties considered are given in table (4.3). The effect of variation in heat conduction coefficient has been studied. The results are shown in fig (4.7) for gas conduction coefficient varying between '1' to '4.35'.

A comparative analysis of fig (4.4), (4.6) and fig (4.7) reveal that the temperature profile is much steeper in case of steel than in case of glass. It is understandable since the major portion of heat transfer is through conduction, and steel has sufficiently larger thermal conductivity as compared to that of glass.

Hollow steel cryochamber (Case III)	
Outer diameter	10.5 mm
Inner diameter	10.3 mm
Length	48mm
Density	7960 kgm^{-3}
Gas conduction coefficient	0.632 $Wm^{-2}K^{-1}$
Thermal conductivity	0.1208 $Jm^{-1}K^{-1}$
Specific heat	500 $Jkg^{-1}K^{-1}$
Emissivity	0.074
Base Temperature	300 K
Detector temperature	77 K

Table (4.3): Dimension and properties of steel cryochamber

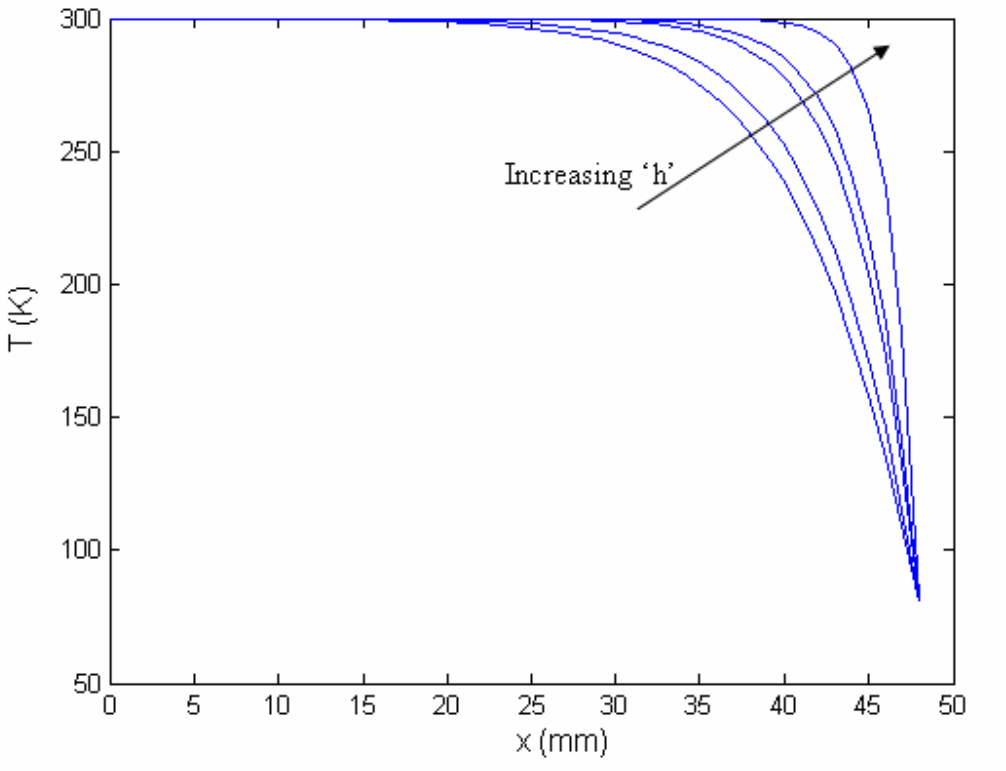

Fig (4.7): Length profile of temperature for various gas conduction coefficients *h* = 0, 0.632, 0.8, 1.0, 4.35 have been studied

The succeeding section deals with the numerical results for the transient case, which is most critical in case of strategic applications, where the cool down time needs to minimum. In this respect, a numerical model which is capable of correctly predicting the cool down time taking into account all the heat transfer modes enables a precise selection of the cryocooler cooling capacity and its cooling characteristics.

4.4.2 Numerical Results: Transient

Considering, a typical case of glass cryochamber having the material and transport properties as given in table (4.1) corresponding to Case- I with cryocooler characteristics given in table (4.4), the time - temperature profile at the detector end was determined.

Cryocooler characteristics (A)	
Cryocooler constant *'a'*	0.039 WK^{-1}
Cryocooler constant *'b'*	-2 W

Table (4.4): Details of cryocooler characteristics given by Kim et.al (5)

In order to check the efficacy of the numerical model developed the first task is to perform the grid convergence check. The grid convergence check is carried out by varying the no. of grids. In the present case the above problem has been solved for case-I with h = 1 $Wm^{-2}K^{-1}$ corresponding to a pressure of 0.9 torr or 6.84 x 10^{-3} Pa employing 48 grids and 96 grids, for a given time step of 1ms and near overlapping temperature profiles have been obtained, as shown in fig (4.8). The slight variation observed is only in the initial few seconds where the fall in temperature is very steep, which is also with in permissible limits.

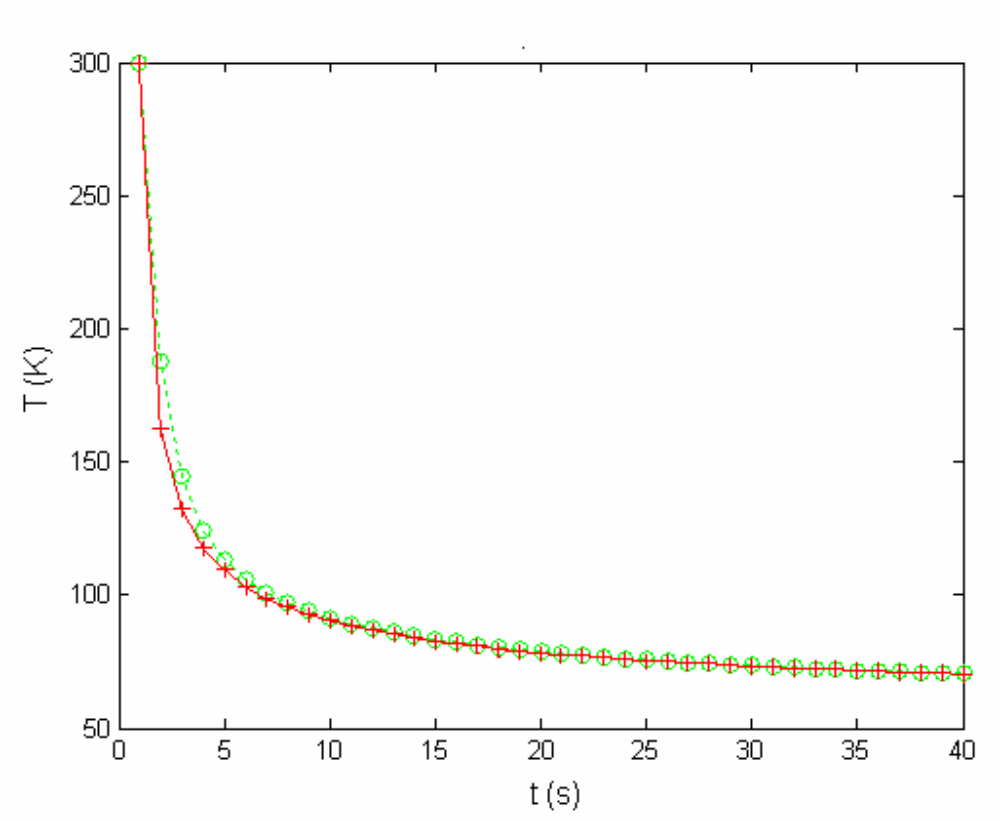

Fig (4.8): Grid convergence check for transient numerical model of cryochamber
Green: 48 grids; Red: 96 grids

In case of transient heat transfer problems apart from grid convergence one needs to check for time step independence as well. Hence, for the same properties and parameters and identical no. of grids i.e. 48 the time step was varied from 5 ms to 1 ms. The predicted temporal variation of temperature at the detector end grid in the two cases is shown in fig (4.9).

It is evident that the plots for the two time steps are nearly overlapping and time step independence for the numerical code is established.

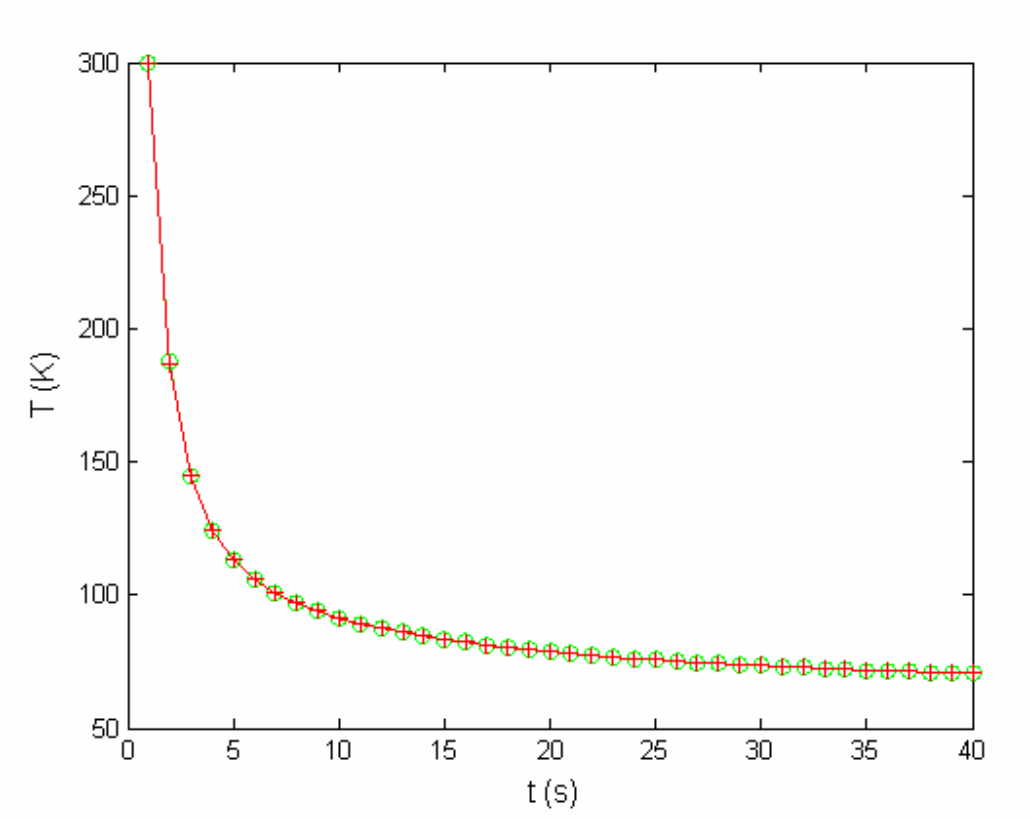

Fig (4.9): Time step independence for transient numerical model of cryochamber
Red: 5ms time step; Green: 1ms time step

After having proved that the predicted results are numerically reliable and unaffected by the choice of number of grids and time step, for the given set of cryochamber parameters it is evident that the cool down time is nearly 27 s. Since, the typical data that has been used is from the data provided by Kim et.al. [5], the predicted cool down time is commensurate with their results.

The numerical model for transient case having been validated was then used to predict the cool down time for the glass cryochamber used in our experimentation, the geometry for which is given in table (4.2). Also, the cryocooler employed in our experimentation has different cooling characteristics [given in table (4.5)] as function of temperature as compared to that assumed in the sample data. The pressure in cryochamber is considered to be 6.84×10^{-3} torr with gas conduction coefficient *(h)* value being 1.0 $Wm^{-2}K^{-1}$.

Cryocooler characteristics (B)	
Cryocooler constant *'a'*	0.009 WK^{-1}
Cryocooler constant *'b'*	0.28 W

Table (4.5): Details of cryocooler characteristics in our case

The emissivity and specific heat values are taken the same as given in table (4.1). The numerically predicted cool down time for this case is shown in fig (4.10).

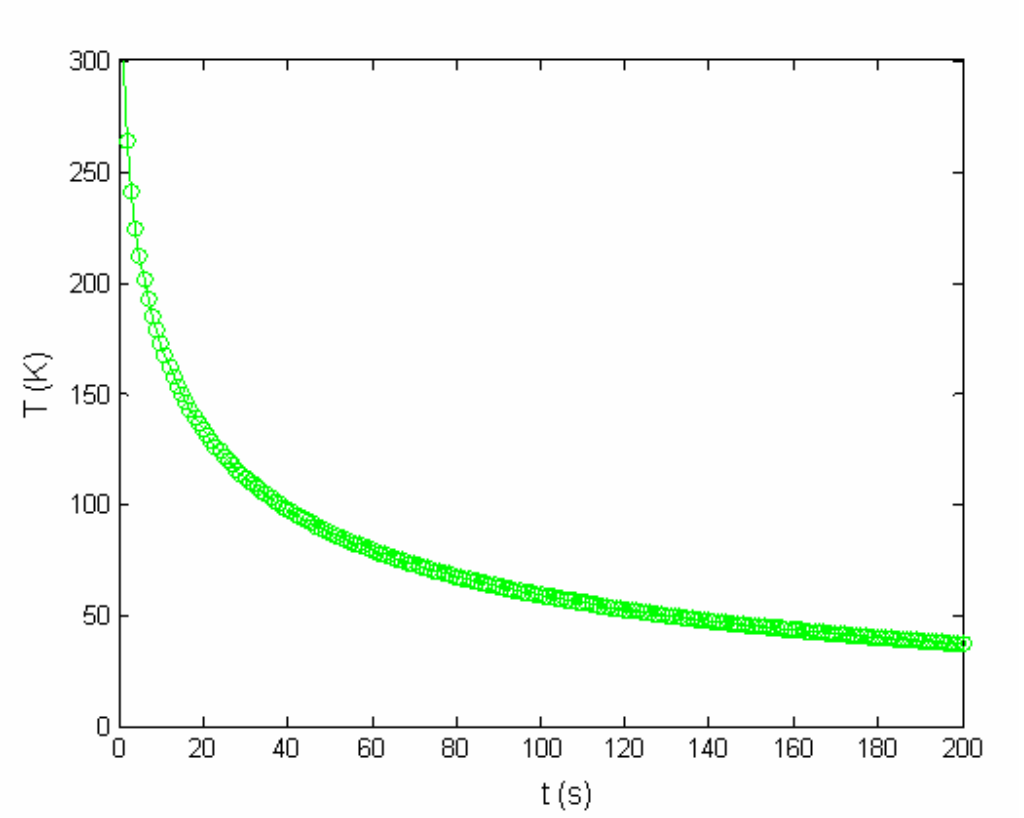

Fig (4.10): Numerically predicted cool down time for Case II cryochamber employing time step of 1ms time

It is evident from fig (4.10) that the cool down time i.e. the time taken to reach the desired temperature of 77 K is nearly 63 s i.e. 1 min 3 s. In case, the cryochamber is operated with the detector in *"bias on"* mode the predicted cooling down time is greater at 85 s or 1 min 25 s as shown in fig (4.11).

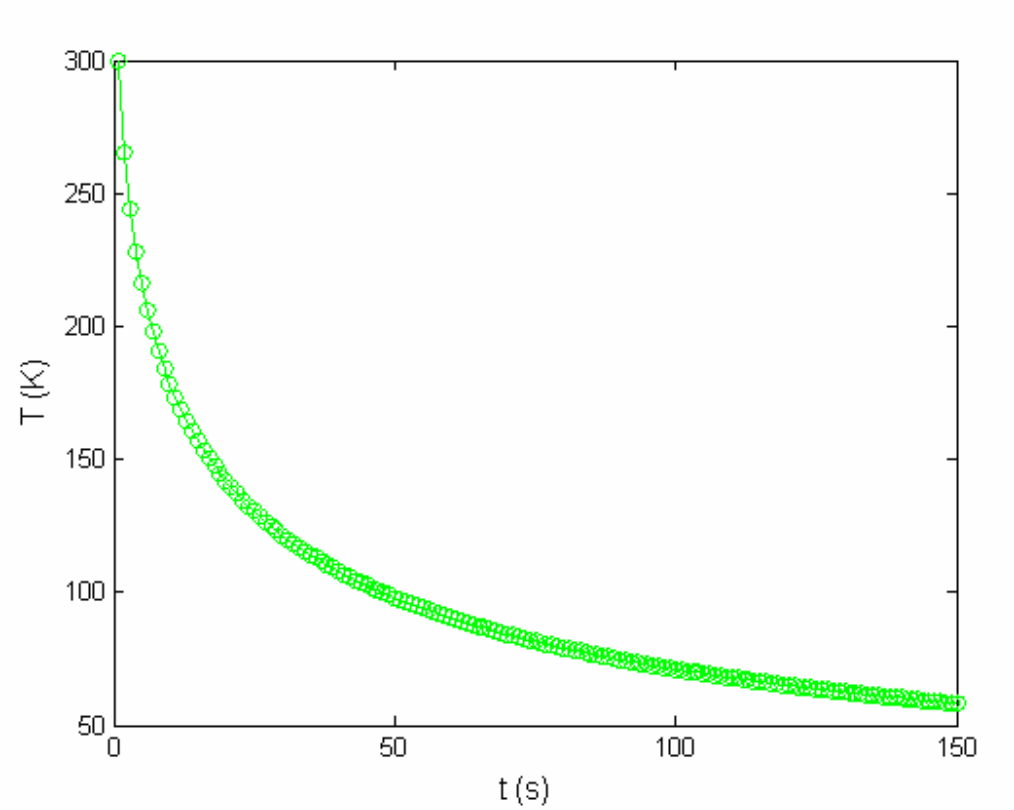

Fig (4.11): Numerically predicted cool down time for Case II cryochamber employing time step of 1ms time in "bias on" detector condition

The length profile of temperature for the case of our cryochamber is shown in fig (4.12). The figure clearly shows the penetration of the temperature changes is ~ 15mm from the cold tip.

Also, the effect of ambient temperature on the cool down time for the detector has also been studied. The temporal variation of cold tip temperature when the starting ambient temperature is 55^{o} C or 328 K is shown in fig (4.13) and (4.14) respectively. The estimated cool down time in "no bias" condition is shown in fig (4.13) and is found to be nearly 75 s or 1 min 15 s which as expected higher as compared to the case when the cryochamber is operated from normal ambient temperature of 300 K. Further, for the case of "bias on" detector condition the cool down time is 98 s or 1 min 38 s and the graph is shown in fig (4.14).

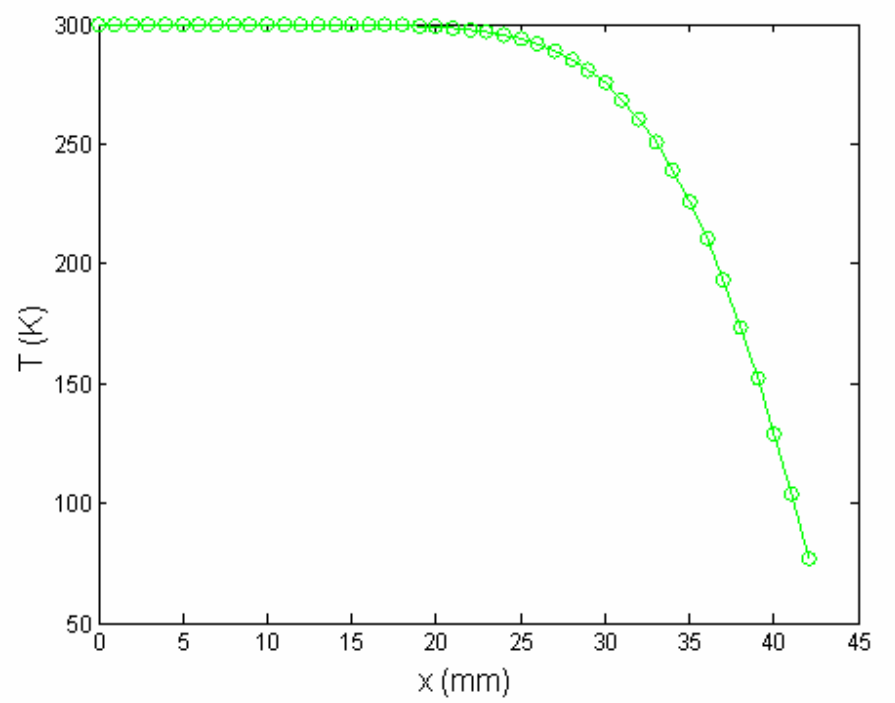

Fig (4.12): Length profile of temperature for Case - II of cryochamber

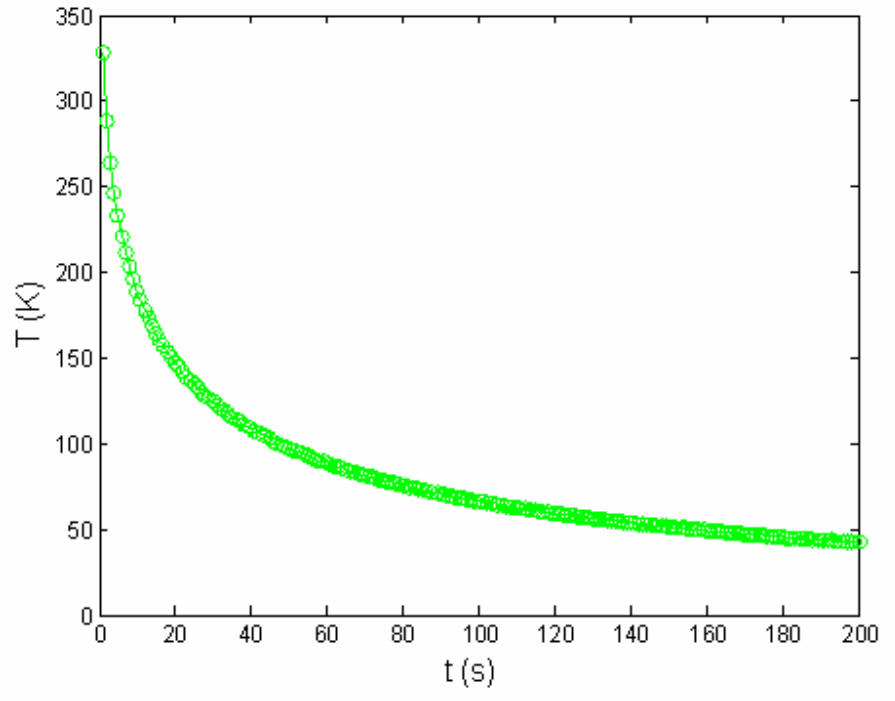

Fig (4.13): Numerically predicted detector cool down time for ambient temperature of 328 K under "no bias" condition

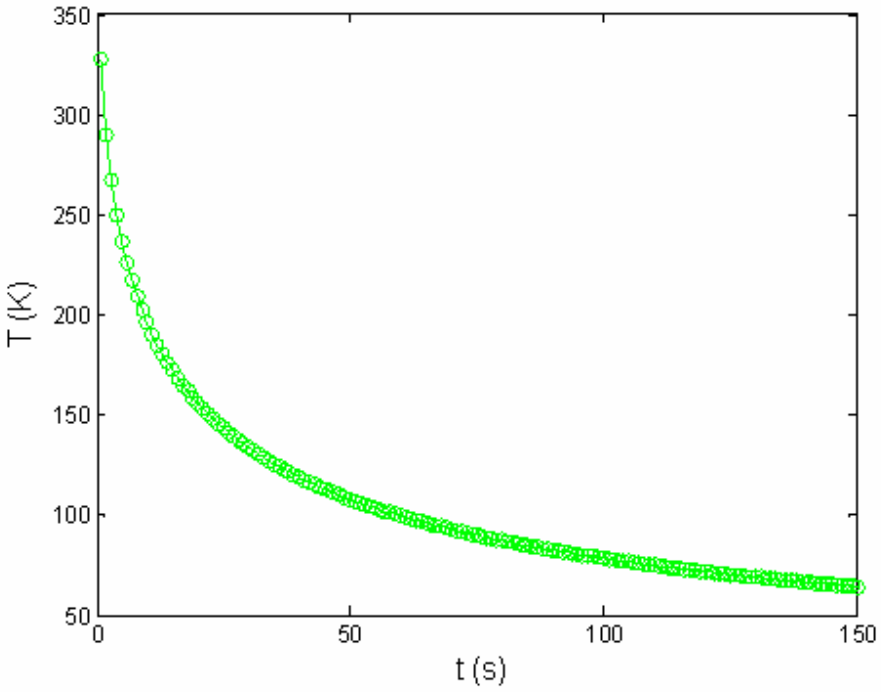

Fig (4.14): Numerically predicted detector cool down time for ambient temperature of 328 K in "bias on" detector condition

Further, variation of ambient temperature has been studied over a range from 150 K to 350 K as well and the cool down time [refer fig (4.15)] has been predicted for two considered thermal conductivities i.e. k = 1.2 $Wm^{-1}K^{-1}$. The cryocooler characteristics used for prediction correspond to Case B. It is observed that the change in thermal conductivity has a significant impact on the detector cool down time. Also, considering that the *thermal penetration depth* is square root function of thermal diffusivity (α) and cool down time $(t_c)$and refrigeration capacity being a linear function of temperature it appears that $t_c \sim k(\rho c)\Delta T^2$ where ΔT is the difference between detector and ambient temperature

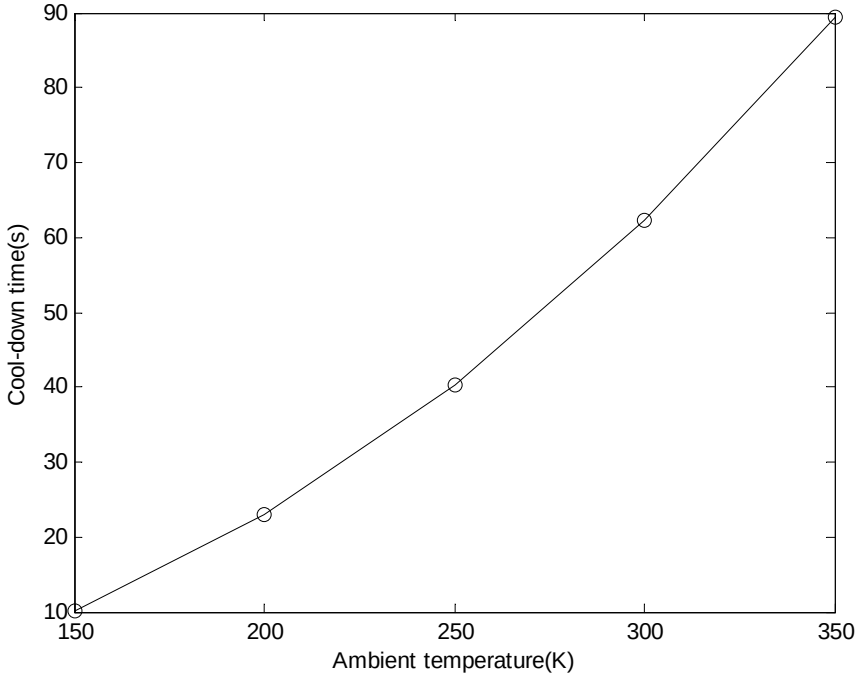

Fig (4.15): Effect of ambient temperature on detector cool down time considered to be operating in "no bias" condition

Another important result that appears from the analysis is that gas pressure has insignificant impact on the cool down time [refer fig (4.16)] contrary to the steady cases. The reason is that the effect of gaseous conduction is limited to a small region close to the cold tip and does not have any significant impact on the cool down time, whereas in steady state case it is entire region that participates, where gas conduction coefficient shows significant impact in terms of existing length profile of temperature. The thermal penetration depth takes approximately 400 s to grow equal to the total length of the bore.

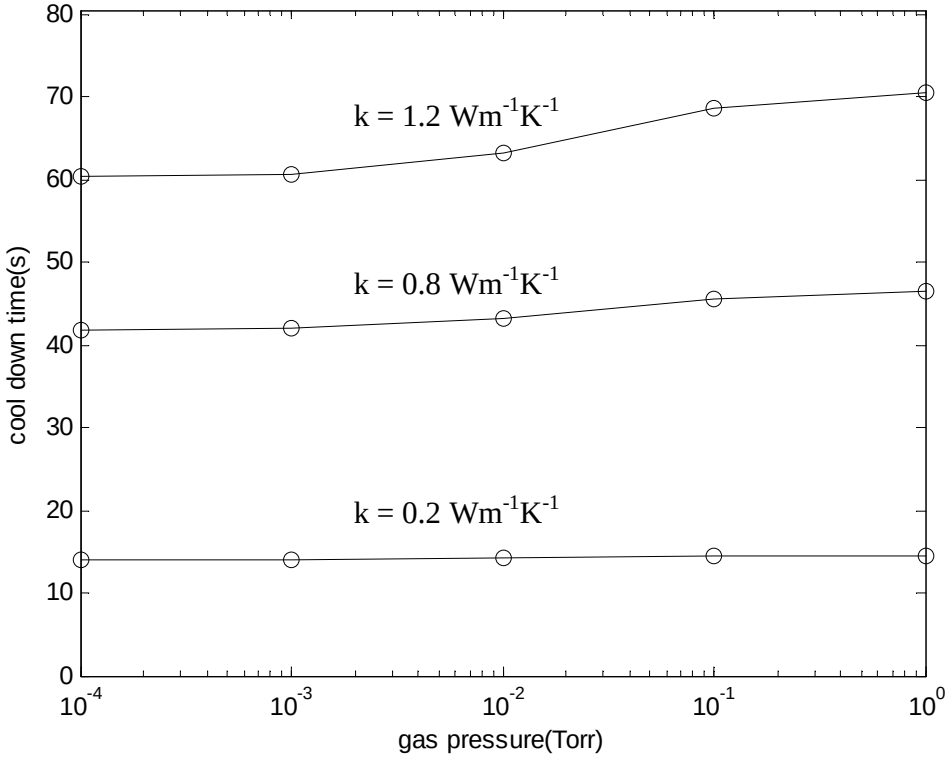

Fig (4.16): Effect of gas pressure variation on detector cool down time

Chapter 5
EXPERIMENTAL VALIDATION

The present problem comprises the study of thermal phenomenon / conditions essential for optimal operation of IR detectors and transducers. The detailed simulation studies given in Chapter-4 for both the various cryochamber configurations provide necessary insight into the various aspects influencing the thermal behavior of the cryochamber. However, in order to be absolutely sure that the developed thermal model is capable of being utilized for practical prediction of thermal behavior of such cryochambers one still needs to carry out sufficient experimentation at least with regards to the cool down time. The validation is all the more essential as there is not much literature available with regards to thermal modeling and hence its comparison with experimental results.

Therefore, in subsequent sections the experimental validation studies carried out on the cryochamber assembly have been discussed and the details of the experimental set up being employed have also been presented. The validation has specifically been carried out for hollow glass configuration with properties corresponding to Case-I utilizing cryocooler characteristics associated with Case –B as detailed in chapter -4.

5.1 Experimental test setup

The configuration of the experimental set up used for the cryochamber experiments carried out for validation of the simulation results is shown in fig (5.1). The main components are; cryochamber assembly with JT cooling provision, high pressure bottle, solenoid and regulation valves and the filter assembly.

The detector inside the infrared detector cryochamber/dewar is cooled to 77K with the help of a Joule Thomson mini-cooler, as shown in fig (5.1), using high pressure nitrogen gas. Both the cool down time and hold on time is observed which should be within specified limits. While cooling the cryochamber, no apparent cooling should take place at its window, which indicates the good health of the cryochamber. In fact to check the health or vacuum stability of the cryochamber the fall in temperature of its window in

a particular time can be observed and compared with the fall in temperature of the window of an unsealed cryochamber under dynamics vacuum.

The relevant details of each of these assemblies are given in the section discussed below.

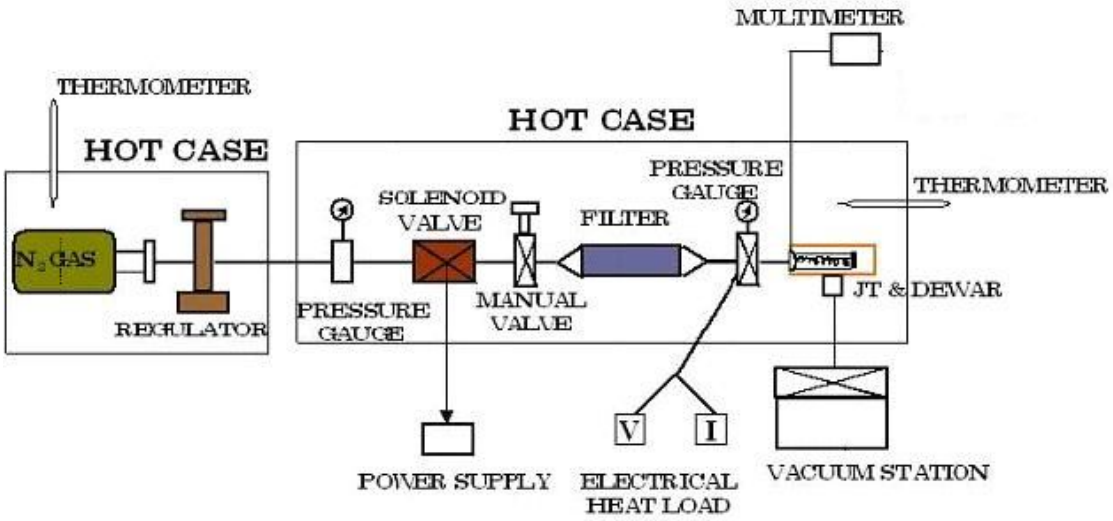

Fig (5.1): Configuration of the experimental setup

5.1.1 Cryochamber assembly and cooling provision

The cryochamber is a hollow glass chamber with internal diameter of 16 mm and an outer diameter of 18 mm and a length of 64 mm. A high pressure nitrogen gas (at 3000 psi) below its inversion temperature of 623 K is expanded through an orifice, causing a drop in temperature due to the adiabatic expansion. This cool, expanded gas cools the incoming gas through a heat exchanger and recuperative cooling occurs, until the liquid is formed.

The heat exchanger is basically made from a fine helically wound finned tube coiled around a mandrel. The heat exchanger must be able to cool the high pressure nitrogen gas say, from 300 K to at least 175 K for liquefaction and achieving maximum efficiency. The heat exchanger should be able to utilize all the cooling effect produced on expansion and raise the temperature of the outgoing gas as near to 300 K as possible.

The functional schematic showing all components and solid sectional view of the cryochamber are shown as fig (5.2a) and (5.2b) respectively.

The cool down time is the time taken to achieve the desired temperature of 77 (when the high pressure gas gets liquefied), from the prevailing ambient temperature. The thermal mass of the Dewar has a major effect on the cool down time and on the system run time.

Hold on time is defined to be the time duration after which the temperature starts to rise once the gas is cut off the cooler.

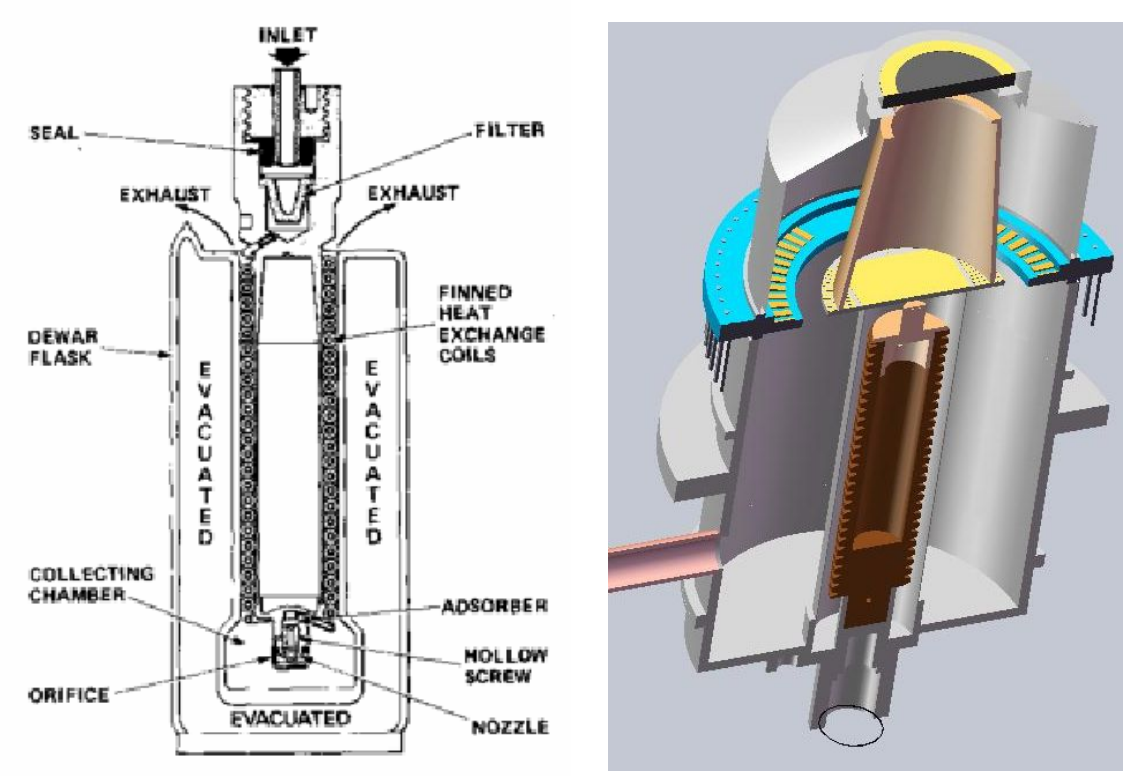

a) Cryochamber functional schematic b) Section view of cryochamber assembly

Fig (5.2): Cryochamber assembly

5.1.2 High pressure bottle

A high pressure bottle is required as storage of high pressure (4500 psi, 254.23 bar) nitrogen gas, which can provide continuous supply of gas for the desired duration of cooling. The bottle shown (make Hymatic, U.K and capacity 2.4 lts) in fig (5.3) is fitted

with an adaptor valve, over which quick release valve can easily be slipped which facilitates easy opening and closing of gas supply from the bottle.

Fig (5.3): High Pressure Nitrogen Bottle

5.1.3 Solenoid valve:

The solenoid valve, fig (5.4), is provided for the electrical on/off operation of gas supply. After opening the bottle manually, the gas supply can be started by a solenoid valve, allowing remote operation of the system.

Fig (5.4): Solenoid valve

5.1.4 Regulation valve:

The supply pressure of the gas is regulated to the desired value at which the cooling experiment is to be performed. A regulator valve (make Hymatic Redditech U.K.) in fig (5.5) is a must in the pressure circuit so that the gas can be regulated to a fixed pressure and a number of experiments can be repeated on the same value.

Fig (5.5): Regulating valve

5.1.5 Molecular sieve filter:

The gas supplied to the mini-cooler should be of the highest purity as impurities like water vapor, carbon dioxide, hydrocarbon and solid particle may cause a total or partial blockage of the expansion orifice which has a diameter of the order of about 50 μm. The gas is required to meet the following specifications:

Water vapour ≤ 0.5 ppm

Carbon dioxide ≤ 1 ppm by weight

Hydrocarbons ≤ 1 ppm by weight

Solid particles ≤ 5 microns size

In order to ensure the purity of the gas a molecular sieve filter is incorporated in the pressure line. It is basically a metal filter with pore size less than 5 microns.

The photograph of the integrated experimental set up used for validations experiments is shown in fig (5.6).

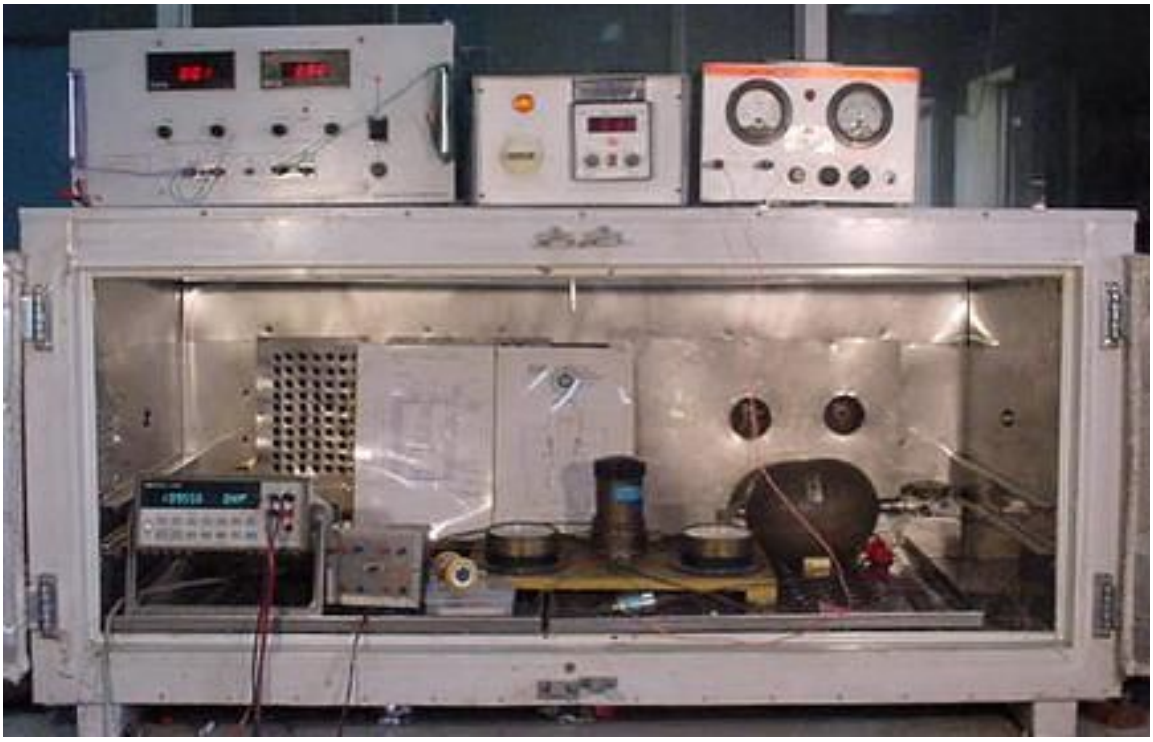

Fig (5.6): Photograph of experimental test setup

5.2 Cooling experiments

The various cryochamber configurations are tested for their performance of cool down and hold on time at typical room temperature for the purpose of validation of the numerical model employing the cooling set up shown in fig (5.6).

The foremost task is to fill the high pressure gas bottle with high purity nitrogen gas to about 4000 psi with the help of a booster. This high pressure gas bottle is then connected to the testing circuit and the gas is regulated to 3000 psi (206.8 bar) with a line regulator. The solenoid valve is subsequently opened electrically so that the high pressure gas is expanded through a small orifice of the cooler, producing cooling due to Joule Thomson effect.

In the absence of the actual device, a temperature sensor called RTDS (Resistance Temperature Dependant Sensor) or a silicon diode is mounted in the dewar at the place of device so that the temperature inside can be measured. Similarly, a small heater is also mounted near the RTDS or silicon diode to simulate the heat load of the actual device, which is typically 50-150 mW. The readings of the fall in resistance of the RTDS or increase in voltage of silicon diode sensor with the fall in temperature are measured with the help of a multi-meter, using a 4-wire system to eliminate the lead resistances.

Once the cooling is achieved to ~ 77 K, certain time is allowed to elapse for the temperature to stabilize, thereafter, the gas supply is cut-off from the solenoid valve, and the hold on time is noted.

The experiments are repeated in the same set-up and with same parameters to check their repeatability. the experiments are also carried out at elevated ambient temperature of 55°C, by keeping the system in a controlled hot air oven.

5.3 Result and discussion

A number of experiments were carried out on this cooling set up and the results are summarized in the tables 5.1, 5.2, 5.3 and 5.4 (details given in Appendix – C).

In table (5.1) below, the comparison of cool down time of different dewar cooler combinations are shown at room temperature without device heat load of 150 mw. The cooling curve for such experiment is shown in fig (5.7).

S.No	Ambient temperature	Heat Load	Cool Down Time
1.	25^{o} C	Nil	1min 05 s
2.	25^{o} C	Nil	1min 03 s
3.	25^{o} C	Nil	1min 05 s

Table (5.1): Cool down time of at ambient temperature without heat load (Regulated pressure used = 206.8 bar or 3000 psi)

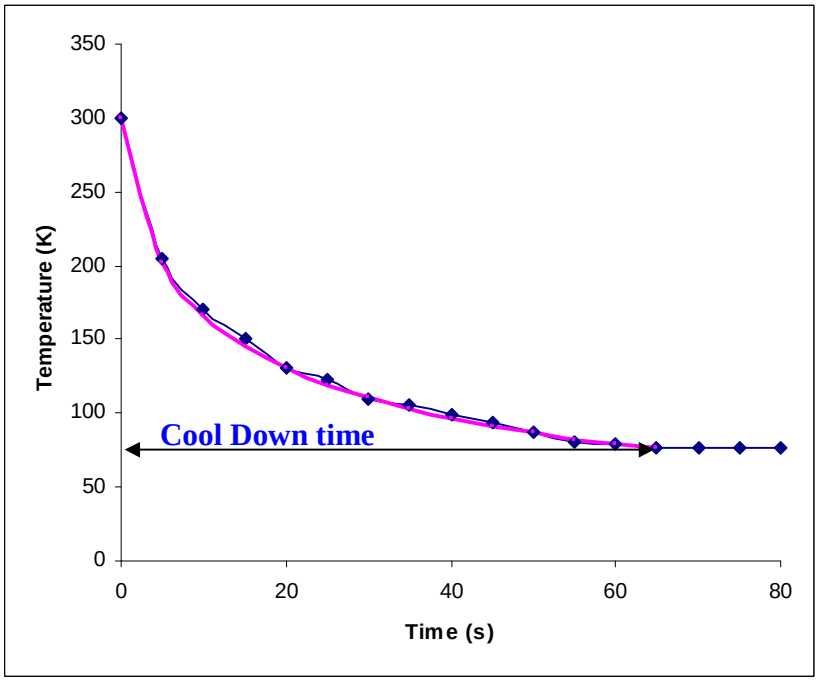

Fig (5.7): Cryochamber cooling curve at 25°C without heat load (Blue: Experimental; Magenta: Numerical simulation)

The numerical results are experimentally validated employing the cryochamber-cooler combinations hardware and the observed cool down time i.e. the time taken to

reach the desired temperature of 77 K is nearly 65 s i.e. 1 min 5 s. The simulation curve is superimposed and the predicted cool down time is nearly 63 s i.e. 1 min 3 s [also see fig (4.10)].

In table (5.2) below, the comparison of cool down time of different dewar cooler combinations are shown at room temperature with device heat load of 150 mW. The typical experimentally observed cool down time value is around 1 min 25 and matches with the predicted simulation value of 1min 25 s. The cooling curve for such experiment is shown in fig (5.8).

S.No	Ambient temperature	Heat Load	Cool Down Time
1.	25^{o} C	150mW	1min 25 s
2.	24^{o} C	150mW	1min 24 s
3.	25^{o} C	150mW	1min 25 s

Table (5.2): Cool down time of cryochamber at ambient temperature with heat load (Regulated pressure used = 206.8 bar or 3000 psi)

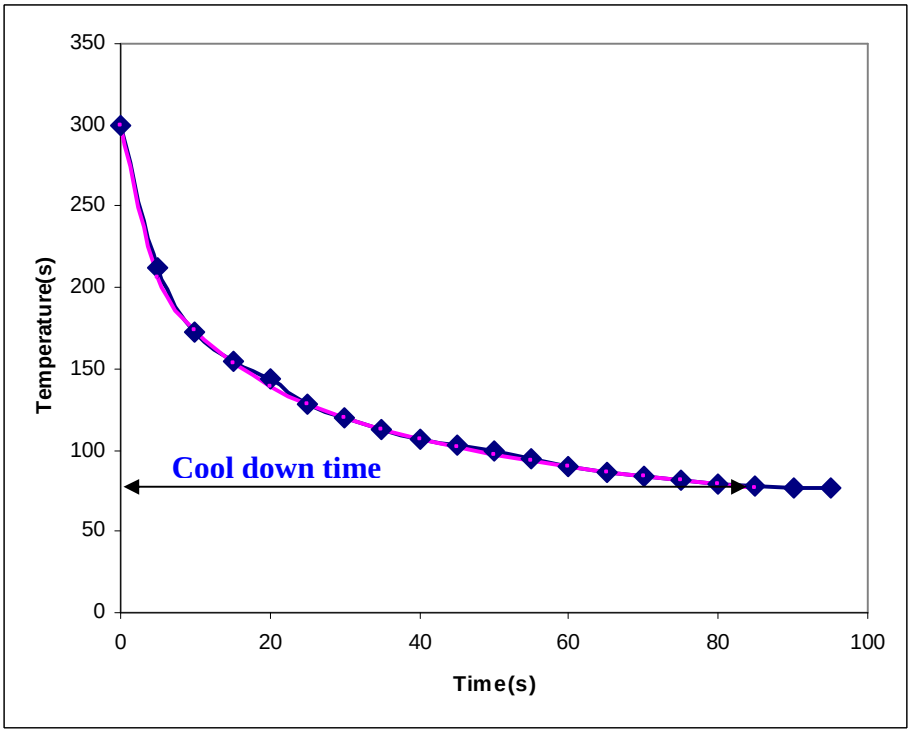

Fig (5.8): Cryochamber cooling curve at 25°C with device heat load (Q_{bias}=150mW) (Blue: Experimental; Magenta: Numerical simulation)

In table (5.3) below, the comparison of cool down time of different dewar cooler combinations are shown at elevated temperature of 55°C without device heat load of 150 mW. The typical experimentally observed cool down time value is around 1 min 20 s against a predicted simulation value of 1min 15 s. The cool down graph for such experiment is shown in fig (5.9).

S.No	Ambient temperature	Heat Load	Cool Down Time
1.	54^{o} C	Nil	1min 18 s
2.	55^{o} C	Nil	1min 20 s
3.	55^{o} C	Nil	1min 20 s

Table (5.3): Cool down time of cryochamber at 358 K without heat load (Regulated pressure used = 206.8 bar or 3000 psi)

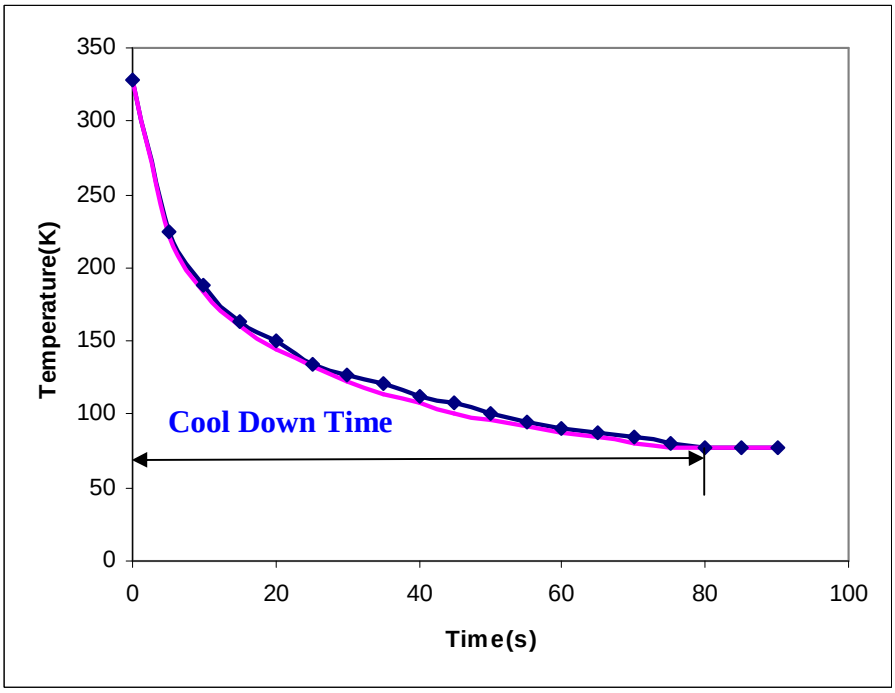

Fig (5.9): Cryochamber cooling curve at 358K without device heat load (Blue: Experimental; Magenta: Numerical simulation)

In table (5.4) below, the comparison of cool down time of different dewar cooler combinations are shown at elevated temperature of 55°C with device heat load of 150 mW. The typical observed cool down time value is around 1 min 40 s against a predicted simulation value of 98 s. The cool down curve for such experiment is shown in fig (5.10).

S.No	Ambient temperature	Heat Load	Cool Down Time
1.	55^{o} C	150mW	1min 40 s
2.	54^{o} C	150mW	1min 37 s
3.	55^{o} C	150mW	1min 40 s

Table 5.4: Cool down time of cryochamber at 358 K with heat load (Regulated pressure used = 206.8 bar or 3000 psi)

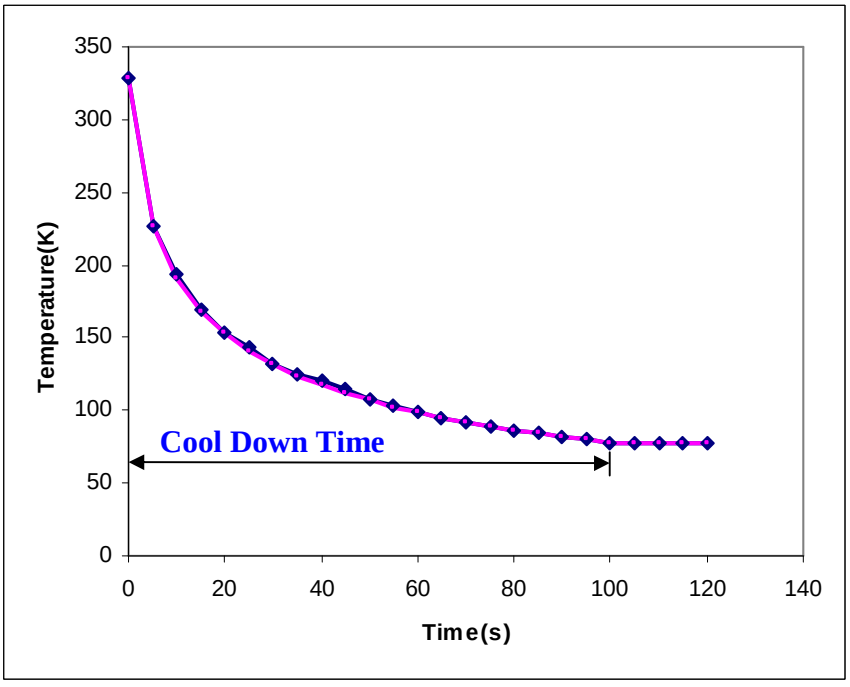

Fig 5.10: Cryochamber cooling curve at 358 K with device heat load (Q_{bias}=150mW) (Blue: Experimental; Magenta: Numerical simulation)

Chapter 6
CONCLUSIONS

Present work involves a thorough study of thermal conditions and phenomenon essential for optimal operation of IR detectors. An overall qualitative analysis of the design considerations of a cryochamber / Dewar housing these IR devices has been carried out which include; mechanical design considerations, need of vacuum integrity, applicable refrigeration systems. Further, finite volume analysis for better comprehending the thermal phenomenon arising in the cryochamber has also been carried out. The modeling results have been subsequently validated through experiments on similar systems to establish its efficacy.

Since analytical methods involve use of error function which is highly computationally intensive, therefore, a generalized numerical approach has been used for both steady and transient thermal analysis.

The basic algorithms for solution of steady state and transient state cryochamber heat transfer problem were developed and the programs for both the cases were made in MATLAB.

The thermal modeling of the cryochamber has been carried out for both steady state as well as transient conditions and efficacy of numerical model was checked by performing check for grid convergence and time step independence.

It is evident from fig (4.10) that the cool down time i.e. the time taken to reach the desired temperature of 77 K is nearly 63 s i.e. 1 min 3 s. In case, the cryochamber is operated with the detector in *"bias on"* mode the predicted cooling down time is greater at 85 s or 1 min 25 s as shown in fig (4.11). The numerical results are experimentally validated with cryochamber cooler combinations and cool down time i.e. the time taken to reach the desired temperature of 77 K is nearly 65 s i.e. 1 min 5 s. The cool down time in case when the cryochamber is operated with the detector in *"bias on"* mode i.e. heat load of 150mW is 85 s or 1 min 25 s and completely matches with numerical result.

Also, the effect of ambient temperature on the cool down time for the detector has also been studied. The estimated cool down time in "no bias" condition temperature when the starting ambient temperature is 55^{o} C or 328 K is found to be nearly 75 s or 1 min 15s

which as expected is higher as compared to the case when the cryochamber is operated from normal ambient temperature of 300 K. Further, for the case of "bias on" detector condition the cool down time is 98 s or 1 min 38 s. The same results in case of experimentation performed with cryochamber cooler combinations were 80 s or 1 min 20s in case of "no bias" and 100 s or 1min 40s cool down time in case of "bias on" detector condition i.e. with heat load of 150 mW.

Hence, it is evident that the numerical formulation correctly predicts the cool down time with an observed maximum error of nearly 6%

The major conclusions that can be drawn from the voracious numerical simulation carried out using the developed model:

- The gas conduction coefficient is essentially a function of pressure inside the cryochamber and is found to increase with increase in pressure
- Gas conduction coefficient shows significant impact in terms of existing length profile of temperature in steady state cases
- Length profile of temperature is much steeper in case when cold well is made of steel than when it is made of glass.
- The estimated cool down time in "no bias" condition is lesser as compared to the case when the cryochamber is operated in "bias on" condition at the same temperature.
- The estimated cool down time in "no bias" condition is found to be higher when the starting ambient temperature is 55^{o} C or 328 K as compared to the case when the cryochamber is operated from normal ambient temperature of 300 K.
- It is observed that the change in thermal conductivity has a significant impact on the detector cool down time.
- Gas pressure has insignificant impact on the cool down time [refer fig (4.15)] in transient cases contrary to the steady cases.

Chapter 7

RECOMMENDATIONS FOR FUTURE WORK

The performance and operation of infrared detectors is affected primarily by two main components,

i) Material, thermal behavior of a vacuum sealed cryochamber

ii) Cryocoolers and their characteristics; Joule Thompson, Stirling etc.

The first part has been thoroughly analyzed both numerically as well as experimentally as part of the present work. One area of work that may be carried out in future in this aspect is experimentation related to metal cryochambers. Although, the results for metal cryochamber can be predicted employing the present code, the experimentation is yet to be carried out.

Moreover, the second part pertaining to cryocooler has sufficient scope for future analysis. The first step is to develop a detailed analytical model specific to the needs of the infrared detector and the cryochamber. The analytical design may then be first verified using voracious numerical simulation. The numerical analysis will enable refine the design of a customized cryocooler with desired cryocooler characteristics. This is especially true for the case of development of Joule Thompson cooler, which is a difficult technology in itself. The predicted results should then be validated experimentally to establish the efficacy of the analytical and numerical codes.

References

[1] J.D.Vincent, “Fundamentals of infrared detectors operation and testing”, John Wiley and sons, 1990.

[2] Stephen Matthews, “Thermal Imaging on the rise”, Laser Focus World, Jan 2004

[3] Sergeant, E.A., “Cryogenics in industry, research and medicine”, Modern Refrigeration Air control, Oct 1996

[4] M.Z. Tidrow, W.R. Dyer “Infrared sensors for ballistic missile defense” Infrared Physics and Technology”, 42 (2001), pp 333-336

[5] C. Boffito, B. Ferrario, L. Rosai, and F. Doni “Gettering in Cryogenic Applications” J Vacuum Science and Technology A, 5(6), 1987, pp 3442-3445

[6] Byung Ha Kang, Jung Hoon Lee, Ho-Young Kim “An experimental study on the cooling characteristics of an Infrared detector cryochamber” Korean journal of Air- conditions and Refrigeration Engineering/ v.16, no. 10, 2004, pp 889-894

[7] Young Min Kim, Byung Ha Kang, “Thermal analysis of a cryochamber for an infrared detector considering a Radiation shield” Korean journal of Air-conditions and Refrigeration Engineering/ v.18, no. 8, 2006, pp 672-677

[8] Young Min Kim, Byung Ha Kang, Seong Je Park “An experimental study on the thermal load of a cryochamber with Radiation shields” Korean journal of Air-conditions and Refrigeration Engineering/ v.20, no. 1, 2008, pp 11-16

[9] Ho-Young Kim, Byung Ha Kang, Dae –Young Lee “A parametric study on the cooling characteristics of an infrared detector cryochamber”, Cryogenics, 40 (2000), pp 779-788

[10] S.V.Patankar, “Numerical Heat Transfer and Fluid flow”, Hemisphere, New York, 1980.

[11] Devienne FM, “Low Density Heat Transfer”, Adv Heat Transfer 1965; 2: 271-356

[12] Springer GS, “Heat Transfer in rarefied gases”, Adv Heat Transfer 1970; 7: 163-218

Appendix -A

MATLAB Program for Steady state case

```
do=input('enter the outer diameter');
di=input('enter the inner diameter');
dx=input('enter the element size');
n=input('enter the number of element');
h=input('enter the gas conduction coefficient');
k=input('conduction coefficient');
e=input('emissivity');
T(1)=input('enter the base temperature');
T(n+1)=input('enter the detector temperature');
for i=2:n
    T(i)=T(1);
end
l=T;
ar=(pi/4)*((do)^2-(di)^2)*1e-6;
for i=1:100000
for j=2:n
ap=(2/(dx*1e-3)^2)+(pi*do*h*1e-3/(k*ar))+((5.67e-8*pi*do*1e-
3)/(k*ar))*(e*4*T(j)^3);
ae=1/(dx*1e-3)^2;
aw=1/(dx*1e-3)^2;
b=((5.67e-8*pi*do*1e-3)/(k*ar))*(e*3*T(j)^4)*(1)+((pi*h*do*1e-
3)/(k*ar))*300+(5.67e-8*pi*do*1e-3*e*(300)^4)/(k*ar);
l(j)=(ae/ap)*T(j+1)+(aw/ap)*T(j-1)+(b/ap);
end
T=l;
end
T
mn(1)=0;
for j=2:(n+1)
    mn(j)=mn(j-1)+ dx;
end
mn;
plot(mn,T)
ylabel('temperature (in K )');
xlabel('distance in (mm)   ');
      hold on
```

Appendix -B

MATLAB Program for Transient case

```
h=input('enter gas conduction coefficient(in W/m.K)');
k=input('enter conduction coefficient(in W/m.K)');
le=input('enter the total length(in mm)');
n=input('enter the number of element');
T(1)=input('enter base temperature(in K)');
T(n+1)=input('enter initial detector temperature(in K)');
ro=input('enter density(in Kg/m^3)');
co=input('enter specific heat capacity(in J/Kg.K)');
do=input('enter outer diameter(in mm)');
di=input('enter inner diameter(in mm)');
em=input('enter emissivity');
dt=input('enter the time interval(in s)');
v=input('enter the number of time interval');
l(1)=T(1);
l(n+1)=T(n+1);
for i=2:n
    T(i)=T(1);
end
dx=0.001*(le/n);

l=T;
nt=T;
ar=(pi/4)*(do^2-di^2)*1e-6;
P=pi*do*1e-3;
alpha=k/(ro*co);
a=alpha/(dx^2);
b=P*h/(ro*co*ar);
ee=(4*P*em*5.67e-8)/(k*ar);
f=a;
g=(h*P)/(ro*co*ar);
u=(P*em*5.67e-8)/(ro*co*ar);
w=1/(ro*co*ar*dx);
o=1;
oo=1/dt;
ntt(o)=T(1);
ddd=300;
for ii=1:v
    i=n+1;
    Tp1=T(i);
    for j=1:100000
        m=l(i);
        if(ddd > 76.9999)
    l(i)=T(i)+f*dt*(T(i-1)-T(i))+ g*dt*(300-T(i))+u*dt*(300^4-Tp1^4)-
w*dt*(0.009*T(i)+0.28);
        else
         l(i)=T(i)+f*dt*(T(i-1)-T(i))+ g*dt*(300-T(i))+u*dt*(300^4-
Tp1^4);
        end
    err=m-l(i);
    if(err < 0.0001)
        break;
    end
```

```
    Tp1=l(i);
    end
    ddd=l(i);
     if(ii==oo+1)
    o=o+1;
    ntt(o)=l(i);
    oo=oo+(1/dt);
    end
    T=l;
    for i=n:-1:2
        Tp1=T(i);
        for j=1:100000
            m=l(i);
        l(i)=T(i)+a*dt*(T(i+1)-2*T(i)+T(i-1))+b*dt*(300-
T(i))+u*dt*(300^4-
             Tp1^4);
        Tp1=l(i);
        err=m-l(i);
        if(err < 0.0001)
            break;
            m=l(i);
        end
        end
        T=l;
    end
end
for i=1:1:(v*dt)
    time(i)=i;
end
T;
ntt;
plot(time,ntt,'k-')
xlabel('Time(in s)');
ylabel('Temperature(in K)');
title('detector temperature vs time');
hold on
```

Appendix -C

COOLING TEST RESULT SHEET -1

Dewar No. : **F-80** Cooler Type. : JT

Experimental Conditions: Sealed Dewar at ambient Temperature 25°C
without Heat Load

Time(s)	Temp(K)
0	300
5	205
10	170.1
15	150.7
20	130.3
25	122.3
30	109.3
35	105.2
40	98.5
45	93.2
50	87.3
55	81.2
60	79.67
65	77.2
70	77.01
75	77.02
80	77.03

Cool Down Time: 65 se

COOLING TEST RESULT SHEET -2

Dewar No. : **F-80** Cooler Type. : JT

Experimental Conditions: Sealed Dewar at ambient Temperature 25°C
with Heat Load= 150mW

Time(s)	Temp(K)
0	300
5	212
10	173.2
15	154.5
20	144
25	128.5
30	120
35	112.5
40	106.5
45	103.5
50	99.5
55	95
60	89.8
65	86.5
70	83.5
75	81.5
80	79
85	78.1
90	77.01
95	77.01
100	77.2

Cool Down Time: 85 secs

COOLING TEST RESULT SHEET -3

Dewar No. : **F-80** Cooler Type. : JT

Experimental Conditions: Sealed Dewar at ambient Temperature 55°C without Heat Load

Time(s)	Temp(K)
0	328
5	225
10	188.5
15	163
20	149.5
25	134.8
30	126.5
35	120.5
40	111.8
45	108.5
50	100.2
55	95.5
60	90.3
65	87.3
70	84.1
75	80.2
80	77.1
85	77.1
90	77.1

Cool Down Time: 80 secs

COOLING TEST RESULT SHEET -4

Dewar No. : **F-80** Cooler Type. : JT

Experimental Conditions: Sealed Dewar at ambient Temperature 55°C
without Heat Load= 150mW

Time(s)	Temp(K)
0	328
5	226.5
10	194
15	169.5
20	153.8
25	143
30	131.8
35	125.2
40	120.2
45	114.5
50	108.2
55	103.5
60	99.5
65	95.2
70	92
75	89.3
80	86.5
85	84
90	82
95	79.8
100	77.5
105	77.1
110	77.05
115	77.02
120	77.05

Cool Down Time: 100 secs